The Switching Behaviour of Single Photochromic Triads studied with Fluorescence Microscopy

Von der Universität Bayreuth
zur Erlangung des Grades eines
Doktors der Naturwissenschaften (Dr. rer. nat.)
genehmigte Abhandlung

von

Johannes Maier
aus Schwabmünchen

1.Gutachter: Professor Dr. Jürgen Köhler
2.Gutachter: Professor Dr. Georg Herink

Tag der Einreichung: 26.02.2021
Tag des Kolloquiums: 18.06.2021

Abstract

Photochromism is the phenomenon that molecules can undergo reversible changes in their structure with light of a specific wavelength. Among a number of photochromic molecules, dithienyl cyclopentene (DCP) is a molecular switch which undergoes a cyclization (ring-closing) reaction upon illumination with light in the ultraviolet (UV) spectral range. The cycloreversion (ring-opening) reaction is accomplished by illumination with light in the visible range. Such photochromic reactions can be useful for the application in two major fields.

The first field is the application in molecular electronics, where their function as a switch can be exploited by designing transistors, gates, logic circuits, or even devices assembled thereof.

The second big field of application is super-resolution microscopy. Special techniques are relying on the digital bright/dark- or on-/off-toggling of the fluorescence of single molecules in the sample in order to identify and localize single molecule fluorescence as single bright spots. Currently, most techniques rely on stochastic molecular processes causing intermittency in single molecule fluorescence. Photochromic switches with their ability to be deliberately switched feature a clear advantage.

In this dissertation, photochromic triads consisting of one DCP and two covalently linked fluorophores, are examined. The triads are tailor-made macromolecules designed in such a way that the state of the switch is monitored by the fluorescence of the fluorophores, which is quenched if the DCP is in its closed state due to an energy transfer from the fluorophores to the photochromic switch.

Monitoring of the fluorescence means the use of confocal fluorescence microscopy in order to reveal the characteristics of the switching processes for ensembles and single triads.

As tens or hundreds of thousand of photochromic triads are present in ensemble samples where the triads are immobilised in a polymer matrix, the fluorescence will decrease exponentially upon UV illumination, and increase with a saturated exponential growth when the UV illumination is ceased and only visible illumination excites the triads to fluorescence, each described by rate equations. This is in stark contrast for the switching of single triads, where a digital change between a highly fluorescent “On”-state and a weakly fluorescent “Off”-state is expected. A summary of those concepts is given, and

additionally an experimental strategy for the switching of single photochromic triads is presented, where the focus lies on a slowed switching reaction. This is achieved making use of special triads and the conduction of experiments at low temperatures.

The slowed reaction at low temperatures is of crucial interest for the experiments presented in two chapters, where the experimental focus lies on the detection of single molecule switching. In the first of these chapters, triads composed of a DCP switch and two strong perylene bisimide (PBI) fluorophores were used. The triads were immobilised in a polymer matrix and cooled down to 10 K. The single triads are initialized in their closed, non-fluorescent state with UV illumination, which is then probed by visible illumination. As the triad will cycle excitation and radiationless decay in its closed form and then, after a statistically distributed time, undergo the cycloreversion reaction, the fluorescence will be delayed with respect to the onset of probe illumination. One measurement contained 400 switching cycles. However, also unavoidable stochastic blinking processes lead to a quenching of the fluorescence of the triads, and obscure the distribution of fluorescence delay times. This is why a control experiment of the same length was conducted and a statistical model of conditional probabilities was applied in order to distinguish between deliberate switching and stochastic blinking presenting the positive predictive value (PPV). It was found that on the average over 15 single triads, the PPV amounts to 0.8 ± 0.1, the probability which can be assigned to deliberate switching rather than blinking for the triads measured.

In the second chapter dealing with single molecule switching, the single molecule measurements were continued with the known triads with PBI moieties as fluorophores, and additionally triads that use boron dipyrromethene (BODIPY) as fluorophores were examined, and as many on-/off-cycles were probed as possible. As a result, the corresponding average PPV for 20 DCP-PBI and 18 DCP-BODIPY triads of 0.7 ± 0.1 is - on the average - the same for both kinds of triads. Furthermore, this PPV was confirmed to be in the same range as for the one in the preceding chapter . In addition, the many repetitions of the measurement pairs switching experiment/control experiment lead to the conclusion that several thousands of switching cycles per triad are possible, showing a remarkably high fatigue resistance of the switching process.

Zusammenfassung

Photochromie nennt sich der Effekt, wenn sich Moleküle abhängig von der Beleuchtung mit Licht bestimmter Wellenlängen reversible Strukturänderungen unterziehen. Innerhalb einer Reihe photochromer Moleküle ist Dithienylcyclopenten (DCP) ein molekularer Schalter, dessen photochrome Reaktion eine Zyklisierung (Ringschlussreaktion) bei Beleuchtung mit Licht aus dem ultravioletten (UV) Bereich des Spektrums ist. Die gegenläufige Zykloreversion (Ringöffnungsreaktion) wird mit Licht aus dem sichtbaren Bereich erreicht. Solche photochromen Reaktionen können nützlich für die Anwendung in zwei großen Feldern sein.

Das erste Feld ist die Anwendung in der molekularen Elektronik, in der ihre Funktion als Schalter für das Design von Transistoren, Gattern, logische Schaltungen oder sogar davon zusammengesetzte Apparate ausgenutzt wird.

Das zweite große Anwendungsfeld ist die super-auflösende Mikroskopie (engl. super-resolution microscopy) jenseits der Beugungsgrenze. Spezielle Techniken beruhen darauf, dass die Intensität der Fluoreszenz von Molekülen digital zwischen hell und dunkel beziehungsweise AN/AUS schwankt, um so einzelne Moleküle zu identifizieren und lokalisieren zu können. Aktuell beruhen die meisten dieser Techniken auf stochastischen molekularen Prozessen, die zu den vorübergehenden Dunkelzuständen in der Fluoreszenz einzelner Moleküle führen. Photochrome Schalter mit ihrer Möglichkeit, die Dunkelzustände gezielt herbeizuführen, zeigen hier einen klaren Vorteil.

In der vorliegenden Arbeit werden photochrome Triaden, die aus einem DCP und zwei daran kovalent gebundenen Fluorophoren bestehen, untersucht. Die Triaden sind maßgeschneiderte Makromoleküle, die so synthetisiert sind, dass sich der Schaltzustand des DCP anhand der Fluoreszenz der Fluorophore ablesen lässt, was auf einen Energietransfer von den Fluorophoren zum photochromen Schalter zurückzuführen ist. Die Fluoreszenz wird unterdrückt, wenn sich das DCP in seinem geschlossenen Zustand befindet.

Das Aufnehmen der Fluoreszenz geschieht dabei durch konfokale Fluoreszenzmikroskopie, um die Eigenschaften des Schaltens von Ensembles und einzelner Triaden zu untersuchen. Dadurch, das Zehn- oder Hundertausende Triaden in einer Ensemble-Probe in einer Polymermatrix eingebettet sind, nimmt die Fluoreszenz durch das Schalten exponentiell ab, wenn diese mit UV-Licht beleuchtet wird. Umgekehrt kehrt die Fluoreszenz bei Beleuch-

tung mit sichtbarem Licht mit einem exponentiellen Anstieg zurück, der bei der Anfangsfluoreszenz sättigt. Diesen Zusammenhängen kann man Ratengleichungen zuschreiben und so die Ringschluss- beziehungsweise Ringöffnungsreaktion charakterisieren. In einem deutlichen Gegensatz dazu wird für das Schalten einzelner Triaden ein digitales Schalten zwischen einem "An"- und einem "Aus"-Zustand erwartet. Diese beiden Konzepte werden vorgestellt, genauso wie eine experimentelle Strategie für das Schalten einzelner photochromer Triade. Hier liegt der Fokus auf einem verlangsamten Schaltvorgang, erreicht durch den Einsatz spezieller Triaden und das Durchführen der Experimente bei tiefen Temperaturen.

Ein verlangsamter Schaltvorgang ist eine wichtige Grundlage für die Experimente, die in zwei Kapiteln vorgestellt werden, deren Schwerpunkt auf Messungen zum Schalten einzelner Triaden liegt. Im ersten dieser Kapitel wurden DCP-PBI-Triaden eingesetzt und in einer Polymermatrix eingebettet, die bis auf 10 K abgekühlt wurde. Die einzelnen Triaden werden durch UV-Beleuchtung in ihrem geschlossenen Zustand initialisiert, und dieser Zustand durch Beleuchtung mit sichtbarem Licht untersucht. Da die Triaden Zyklen aus Anregung und strahlungsloser Rückkehr in den Grundzustand durchläuft, wird sie nach einer statistisch verteilten Zeit die Ringöffnungsreaktion vollziehen, sichtbar an Hand eines verspäteten Einsetzens der Fluoreszenz relativ zur Beleuchtung mit sichtbarem Licht. Eine Messung bestand aus 400 Schaltzyklen. Jedoch führen auch unvermeidbare Blinking-Ereignisse zu einem Ausbleiben der Fluoreszenz, die die Verteilung der Einschaltzeiten verfälschen. Deswegen wurden auch Kontrollexperimente durchgeführt und ein statistisches Modell für bedingte Wahrscheinlichkeiten angewandt, um zwischen gezieltem Einschalten und stochastischem Blinking zu unterscheiden. Das Ergebnis dieses Modells ist der positive Vorhersagewert (engl. positive predictive value, PPV), der im Mittel für 15 Triaden bei 0.8 ± 0.1 liegt. Dies ist die Wahrscheinlichkeit, die mit gezieltem Schalten statt Blinking für die vermessenen Triaden verknüpft werden kann.

Im zweiten Kapitel mit Einzelmolekülmessungen wurden die Messungen an einzelnen Molekülen fortgeführt, diesmal mit den bekannten Triaden mit den PBI-Fluorophoren und zusätzlich mit Triaden, bei denen statt des PBI als Fluorophore Bor-Dipyrromethene (BODIPY) als Fluorophore kovalent gebunden wurden. Es wurden so viele AN-/AUS-Zyklen wie möglich aufgenommen und als Ergebnis für beide Arten von Triaden im Mittel ein PPV von $0,7 \pm 0,1$ berechnet. Dabei wurden 20 DCP-PBI Triaden und 18 DCP-BODIPY Triaden untersucht. Die vielen Wiederholungen der Paare Schaltexperiment/Kontrollexperiment lassen den Schluss zu, dass sich einzelne Triaden mehrere tausend Male schalten lassen, eine bemerkenswert hohe Dauerfestigkeit.

Contents

List of abbreviations

APD avalanche photo diode

BER bit-error-ratio

BODIPY boron dipyrromethene

DCP dithienyl cyclopentene

NA numerical aperture

OD optical density

PBI perylene bisimide

PMMA poly(methyl methacrylate)

PPV positive predictive value

SIL solid immersion lens

UV ultraviolet

WFL wide-field lens

List of Figures

List of Tables

1. Introduction

Photochromic molecules can undergo a reversible change in their structure upon illumination with light of a specific wavelength [1, 2], accompanied by a change in their spectral characteristics. Their capability of taking different states triggered by an external stimulus makes them promising candidates for the application in two major fields.

In super-resolution imaging, photochromic molecules can help to push the optical resolution limit to some 10 nm, opening a field of applications in life sciences and materials sciences [3, 4].

Techniques like stochastic optical reconstruction microscopy (STORM) [5] and photoactivated localization microscopy (PALM) [6] rely on a stochastic on/off-toggling of the fluorescence of single molecules, in the latter case even caused by an additional light stimulus. Other techniques like stimulated emission depleption microscopy (STED)[7–9] and ground state depletion microscopy (GSD) [10] make use of molecules which can undergo transitions to non-emitting states by the saturation of fluorescence transitions (RESOLFT principle, reversible saturable optical linear fluorescence transitions)[11]. One further development is the MINFLUX technique, with its capability of achieving nanometer resolution with low photon fluxes [12].

The fact that photochromic molecules can undergo changes between a dark and a bright state upon illumination with light, not purely relying on stochastic processes, grants them outstanding properties for applications in super-resolution microscopy [4, 13, 14]. So far, an optical resolution of 75 nm was demonstrated in RESOLFT microscopy with carboxylated photoswitchable diarylethenes on tubulines and nuclear core complexes [15].

The importance of pushing the resolution limit further and further to smaller scales was emphasized and acknowledged in 2014 with the Nobel Prize in Chemistry for Betzig [16], Hell [17], and Moerner [18].

The second big field of application is that of molecular electronics, where photochromic organic molecules can serve as optical switches, by the way serving the continuous strive for miniaturization in electronics. Contemporary sizes of silicon semiconductor technologies are 7 nm [19], fabricated with extreme ultra-violet (EUV) lithography, whereas the size of organic macromolecules is typically in the range of some nanometers [20].

The two key functionalities of a transistor have been demonstrated by making use of the

switchable fluorescence of an ensemble of photochromic triads [21–24]. Such a transistor runs with photons instead of electrons, but shows the typical characteristics also an electronic transistor features. Firstly, a small current of ultraviolet (UV) photons can control a large current of fluorescence photons, which is known as the amplification feature in electronics. Secondly, the ability to switch between a high and a low state of fluorescence corresponds to the transistor as a digital switch in logic operations [25–29]. This opens the field of applications in molecular electronics [30], enabling the switching of energy transfer and conductance [31–33], the switching of a fluorescence signal in a smart matrix [34], or memory applications based on photochromic switches [35–40]. Speaking of the above-mentioned functionalities as ”basic circuits” in molecular electronics, devices can be designed which find application in logic gates [41] as well for safety purposes [42, 43], and also rewritable paper was developed [44]. Apart from these electronic applications, also macroscopic properties could be manipulated, like liquid-crystal phase changes [45–47] or crystalline states [48, 49] which led to the design and development of molecular machines [50–52]. In 2016, Sauvage [53], Stoddart [54] and Feringa [55] were awarded with the Nobel Prize in Chemistry for the design and synthesis of molecular machines.
This is why photochromic materials might contribute with huge benefits in life sciences, engineering, and materials sciences, and are mentioned (next to electro- and thermochromism) as ”Smart Materials” in an anticipatory report on the consequences of technologies (ger. ”Technikfolgenabschätzung”) for the German federal parliamant [56].
For all these applications, the switching of single photochromic molecules became a highly interesting topic [57]. The switching of single molecules has been demonstrated in several publications, where the principle experiment was done by comparing images before and after UV and visible illumination, resulting in images with no or low fluorescence and images with bright fluorescence, respectively [58–60] and again by reading out the times of low and bright fluorescence after UV and visible illumination, respectively [59, 60]. Other experiments show the influence of the UV stimulus on the fluorescence transients of single photochromic molecules: upon UV illumination, the distribution of On- and Off-states regarding fluorescence changes to more Off-states [61], however leaving the influence of unavoidable blinking of single molecules uncertain.
This dissertation reports on how to experimentally find a way to demonstrate the switching of single photochromic triads consisting of one dithienylcyclopentene DCP switch and two fluorophores by evaluating influencing parameters like temperature and the unavoidable blinking [62–64] present in the fluorescence of single molecules embedded in a matrix. For such triads, the state of the DCP can be monitored via the fluorescence of the fluorophores.

- Chapter 2 starts with an overview over photochromism and its historical background, then introducing photoswitches in general, and DCP in particular. A brief over-

view over the synthesis and functionalization strategies is given, as well as a short introduction to the switching process itself.

- In Chapter 3, at first the concept of photochromic triads is presented and especially the structures of the triads used for the experiments in this dissertation are shown. These triads have already demonstrated their switching behaviour as transistors [21] and in optical gating [22, 25], and an overview of these publications is given. As these experiments all report on the switching behaviour of ensembles of photochromic triads, the demonstration of switching at the single molecule level is an obvious goal to pursue. To achieve this goal, the photohpysical process of blinking, which will also be covered shortly, must be taken into account, as well as the work that has already been done on photochromism at the single molecule level by Irie et al. [58–61]. It then illustrates the experimental way which is chosen to detect the switching of single photochromic triads. It follows the strategy to slow down the process by changing two parameters. A first point is the introduction of triads that are expected to undergo a slower switching reaction, which were provided by the workgroup of Prof. Dr. Mukundan Thelakkat. A second point is the strategy of cooling the sample to low temperatures, which is based on preliminary works [65, 66] showing a large decrease in the switching reaction, making it slow enough for the detection in single molecule experiments. It is then followed by the mathematical description of typical experiments on ensembles [25, 66], which serves as a reference, and the measurement strategy for single molecule switching and the mathematical description for the interpretation of the results.

- A summary of the sample preparation as well as the presentation of the experimental setup is then given in Chapter 4. The experimental setup is a home-built fluorescence microscope with a special feature, a solid immersion lens (SIL) objective, which is necessary to detect the signals from single emitters at low temperatures. The application of this concept [67–69] is summarized and presented here, as well as the typical operation parameters for the cryostat. It is directly followed by the Chapters dealing with the measurements and results.

- Based on the prework described in Chapter 3, the temperature for all experiments in Chapters 5 and 6 was fixed to 10 K, and experiments on single triads consisting of a DCP and two perylene bisimide (PBI) fluorophores, were carried out in order to study the influence of blinking and the statistical nature of the onset of fluorescence after UV illumination. Here, with introducing a statistical model based on conditional probabilities, the positive predictive value (PPV) for the switching of single photochromic triads provides information on the reliability of the switching.

It is the probability that a triad shows deliberate light-induced switching rather than stochastic blinking. The average PPV of 15 triads measured was found to be 0.8 ± 0.1. For one triad with a high PPV of 0.964, the dependence on the intensity of the probe beam was also studied, showing only a weak variation between 0.958 and 0.965 for varying the intensity between 60 W/cm^2 and 200 W/cm^2.

- These results were further confirmed in Chapter 6, where, in addition to the study of the fatigue resistance of the triads, i. e. the number of cycles a triad can withstand, a second kind of triad was introduced with boron dipyrromethene (BODIPY) as a fluorophore. It was found that triads can withstand some thousands of switching cycles (accumulated illumination time of hours both for visible probe light and UV cyclization light) without seeing a dramatic change in the positive predictive value. Another result is the fact that for both kinds of triads, DCP-PBI and DCP-BODIPY, the average PPV amounts to 0.7 ± 0.1, a value which is clearly too low for memory applications, yet well-suited for application in super-resolution microscopy. By introducing another model it is shown that with a PPV of only 0.7, i. e. the probability that the return of fluorescence after illumination with UV light is indeed due to switching rather than blinking, an ensemble of only 12 triads can enhance the probability that at least one triad exhibits a switching signal to 0.999 999, or vice versa, a bit-error-ratio (BER) of only 10^{-6}. These small ensembles still feature small sizes and thus can serve the strive for miniaturization in electronics.
  In Chapter 7 the results will be summarized and brought into context, illustrating the way from ensemble experiments to experiments dealing with the switching of single photochromic triads.

2. Photochromism

2.1. Overview over Photochromism

The term “photochromism” refers to the fact that organic molecules undergo a change in their spectral characteristics, i. e. chemical structure, electronic structure, refractive index, absorption and emission spectra, oxidation/reduction potentials, dielectric constant, conductance, solubility, and others, upon excitation of light with a specific wavelength [1, 2, 70–72]. One has to distinguish between photochromism itself, where the change in the spectral characteristics is caused by light in both directions, and effects like thermochromism (heat as stimulus)[73], solvatochromism (spectral characteristics depend on the solvent a compound is dissolved in)[74, 75], or electrochromism (an electric field as the stimulus) [76], to mention only three. For all these other effects the transition between the different states depends on the respective stimulus for at least one direction of the reaction.
Early discoveries on the dependence of characteristics of certain chemical compounds were already made in the 19th century. Fritzsche [77] observed the bleaching of a solution of tetracene in sunlight and the return of colour by night already in 1867. In 1876, ter Meer discovered a reversible colour change in zinc pigments upon illumination with sunlight [78]. Another term “phototropy” (ger. “Phototropie”) was proposed by Marckwald in 1899 [79], by that time the summarizing term for phenomena dealing with the change of chemical compounds upon illumination with light [80].
The term “photochromism” itself was introduced in the 1950s, when photochromic compounds were synthesized by Hirshberg [81–83]. Yet the disadvantage of the components discovered was the lack of thermal irreversibility, obliterating the border between thermochromism and photochromism. A giant step towards thermally irreversible photochromic compounds was made in the 1980s, when Irie and coworkers developed diarylethenes [84, 85]. From then on, the field has grown, and a number of review articles and books on the synthesis [1, 2, 20, 36, 70, 72, 86, 87],have been published, and also for the applications like in single-molecule experiments [57], in super-resolution imaging [3, 4, 13] and applications in devices [20, 72] fields of research have evolved.
The following sections first give an overview over photoswitches, the photochromic switch dithienylcyclopentene used in the experiments for this dissertation in particular, then go

on to characteristics of the dithienylcyclopentene and a short explanation of the switching process of the DCP.

2.2. Photoswitches

One has to differentiate between photochromic systems where both ways of the reaction are caused by light (P-type photochromism), and systems where at least one way of the reaction occurs thermally (T-type photochromism), i. e. in most cases the spontaneous back-reaction under standard conditions, i. e. especially room temperature, when the source of illumination is removed [1, 2].
The following section gives an overview over different photochromic systems, comparing their characteristics, advantages and (possible) drawbacks. For this purpose, requirements are postulated and presented shortly here [2, 88]:

1. Strict priority on light as the only stimulus for both ways of the reaction. This goes along with a high thermal stability of the isomers, as well as the independence from other ambient stimuli (pH value or electric field). Otherwise, the photochromic properties overlap with other effects, namely thermochromism, solvatochromism, and electrochromism, respectively.

2. high photostability and fatigue resistance. A degradation with the probe and/or conversion light need to be excluded. In other words, the number of switching events needs to be high.

3. high sensitivity of the photochromic reaction. First, the quantum yield of the switching reaction should be high, close to 100%, and second, no or at least only little crosstalk between the switching and the probe wavelengths exists. These both characteristics are vital for efficient and reliable switching.

4. a rapid response. The time needed for switching a photochromic system should be short, i. e. in the picosecond time range.

5. reactivity in solid state. Expecially for applications in devices for optical gating [22] or the use as actuators [20], the preparation of photochromic molecules in the solid state (embedded in films, crystallized) is necessary.

2.3. An overview over classes of photochromic switching mechanisms

The following sections shall give an overview over various switching mechanisms of (partially) photochromic molecules. Their features and benefits, yet also their drawbacks concerning the above-mentioned requirements will be discussed. It is only an exemplary list in order to compare different switching mechanisms.

2.3.1. Molecular Switches with Cis-Trans-Isomerization - Azobenzenes and Stilbenes

A class of molecules featuring T-type photochromism is formed by Azobenzenes [89] and Stilbenes [90], where the photochromic reaction is the conversion from a trans- to a cis-isomer of the respective molecule. Figure 2.1 shows, as an example, a simple azobenzene in its cis- (left) and trans-state (right). The reaction from trans to cis can be accomplished with light in the UV range, the backward reaction occurs under illumination with blue light. However, the molecules also return to the trans-azobenzene state in the dark at room temperature, making heat a second trigger for this reaction. It is a transition along the double-bond linking the two nitrogen atoms in the center of the molecule. The same

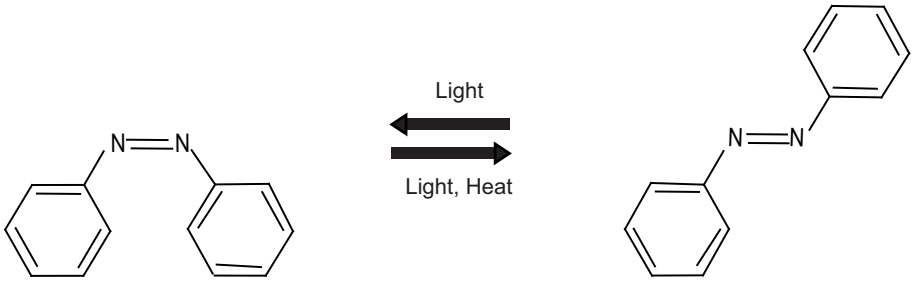

Figure 2.1.: *A molecule of the azobenzene class of molecules in its cis- (left) and trans- (right) state. The molecule undergoes a transition from the trans- to the cis-isomer upon illumination with UV light, whereas the reaction back to the cis-state can be achieved either with illumination with blue light, or in the dark under the influence of heat (or a combination of both).*

mechanism works for stilbenes, where the nitrogen atoms are replaced by carbon atoms [91]. Yet, stilbene can also undergo an irreversible photocyclization reaction [92], which makes them an archetype molecule for the later-discussed diarylethenes [84].
Nevertheless, photochromic reactions which feature a cis-trans isomerization are thermally reversible and therefore not suited for applications which require thermal stability of the states of the photochromic switch.

2.3.2. Molecular Switches with Photocyclization - Stilbenes, Spyropyrans, Diarylethenes

Another class of reactions belonging to photochromism is the one of ring-closing/ring-opening reactions driven by light. Next to the above-mentioned stilbenes, also spyropyrans [93], furylfulgides [94, 95] and diarylethenes [1, 2, 70, 72] undergo such reactions. Figure 2.2 shows the reaction for spiropyran (right) being transformed to merocyanine (left) by light in the UV spectral range. Again, the reaction back to spiropyran is also driven by heat, a drawback for the requirement of thermal irreversibility of the photochromic reaction. Based on the disadvantages of thermal irreversibility and low fatigue resistance of other

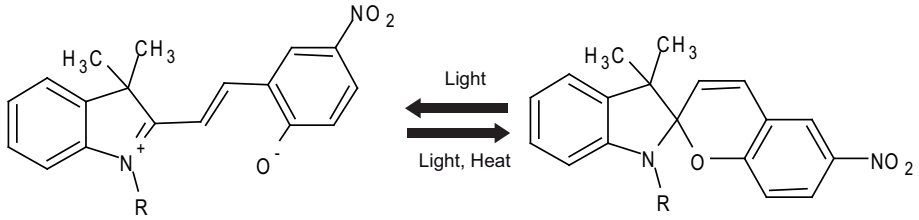

Figure 2.2.: *A spiropyran molecule (right) can be converted to merocyanine with light in the UV spectral range, whereas the reaction back to spiropyran can also be driven by heat. Spiropyran is an example for a molecule undergoing a ring-opening/ring-closing photoisomerization reaction.*

molecules, diarylethenes came into focus for the development of photochromic switches.

2.4. Diarylethenes

Figure 2.3 a) shows the photochromic switch *1,2-bis(2-methyl-5-phenyl-3-thienyl)perfluorocyclopentene* [21], which is a well-known switch from the diarylethene family and called DCP (for *dithienylcyclopentene*) hereafter. The switching happens as a cyclization reaction upon illumination with UV light (see blue arrow with the respective wavelength of 325 nm and the assigned rate of the reaction k_{oc}, Figure 2.3 a), top).

The switch can return to its open state by illumination with visible light (see green arrow with the respective wavelength of 488 nm and the assigned rate k_{co}, Figure 2.3 a) bottom). Concerning the absorption spectrum shown in Figure 2.3 b), the switching can be assigned to different spectral features for the open and the closed conformations of the DCP. In its closed state (blue line) the DCP absorbs light in the UV range from 280 nm - 400 nm and additionally, light in the visible range from 450 nm - 700 nm. For the open state of the DCP, the UV absorption band is narrower, between 280 nm - 350 nm, and the band in the visible range is not present anymore. Thus, the switching process can be assigned to the

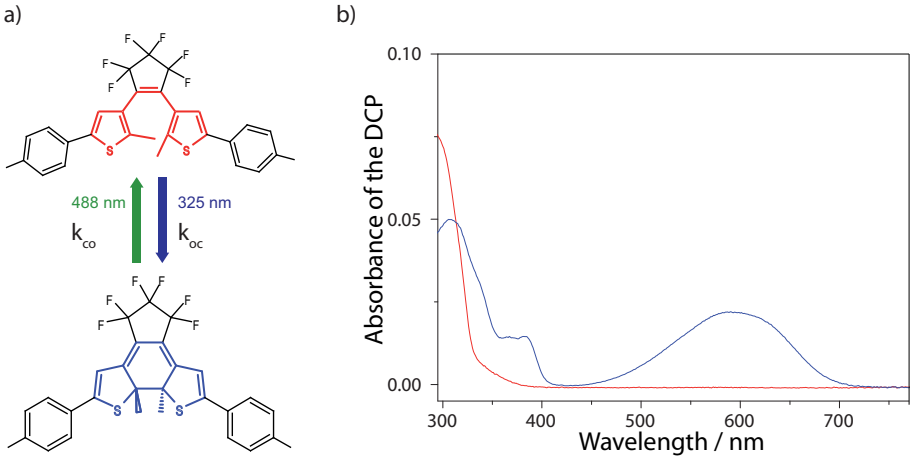

Figure 2.3.: *a) The dithienylcyclopente molecular switch with its open (top) and closed (bottom) state. The closed state is reached by illumination with light in the UV range, in this case* 325 nm*, and the ring-opening reaction is achieved by light in the visible range, here* 488 nm*. The assigned rates k_{co} and k_{oc} are the rates for the close-to-open reaction and for the open-to-close reaction, respectively, and depend on the intensity of the respective illumination wavelength. b) The absorption spectra of the closed (blue line) and the open (red line) state of the DCP switch, measured in toluene solution. The closed state features two absorption bands, one in the UV light range, another in the visible range, whereas the open state of the switch only absorbs light in the UV spectral range. Adapted from [69]*

UV absorption feature [21].

2.4.1. Characteristics of Diarylethenes

In order to enhance photophysical stability and thermal irreversibility of the switching, diarylethenes have been designed and constructed as tailor-made molecules with optimized characteristics [36, 85, 96]. By changing the aromaticity of stilbene-like chemical compounds and substituting the phenyl groups by heterocyclic ones, i. e. for example, thienyl groups (see the cyclic groups with sulfur atoms in Figure 2.3 a)) a higher stability with respect to thermal irreversibility and fatigue resistance can be reached theoretically [96] and in the laboratory [84].

Another point is the perfluorination and the size of the cycloalkene ring (see the five-membered perfluorinated ring in Figure 2.3 a)). Syntheses of similar compounds showed that decreasing the size of the perfluorinated ring shifted the maximum of the absorption spectrum from 510 nm for the six-membered to 526 nm for the five-membered and 532 nm for the four-membered ring (another molecule with perfluorinated methyl groups, i. e. no ring structure anymore, has its absorption maximum at 449 nm)[97], yet having a reduced cyclization quantum yield for decreasing the ring size [98]. So, one is faced with two of the above-mentioned requirements here which cannot be fulfilled at the same time. On the

one hand, a high cyclization reaction quantum yield should be present in order to have a high sensitivity of the photochromic reaction. On the other hand, to enhance the reliability of switching, the absorption band in the visible range should be shifted away from the one in the UV range. This way, a crosstalk between switching to the open or closed state, should be diminished. As a reasonable trade-off between these two opposing features, the five-membered perfluorinated ring was recommended [36]. In addition to that, the perfluorination speeds up the switching process [20].

2.4.2. The Switching Process of Diarylethenes

Diarylethene phtochromic switches and their reactions have been widely examined. In this section, the switching process itself shall be discussed briefly as an overview. The potential energy surface for the DCP shows two minima, each for the electronical ground state S_0 and the electronically excited state S_1, see Figure 2.4, corresponding to the closed (left) and open (right) state of the switch. Upon excitation to the excited state S_1, the DCP switch can relax to its ground state S_0 either to the closed or the open conformation. This process is enabled by a so-called conical intersection (see Figure 2.4), which provides the reaction pathway to both the open- and the closed-ring minima in the ground state of the switch [20], a process which was modeled and simulated [99].
From this figure also a thermal component of the switching process can be explained. Being excited with light in the UV range from its open state, the excitation can decay to the conical intersection via internal conversion, and further to the closed isomer minimum in the ground state in another radiationless process [20]. On the other hand, if the switch is excited from its closed state with visible light, the energy barrier between the two minima in the potential energy surface S_1 needs to be overcome to reach the conical intersection. Here, in summary, two possibilities are present. Either the excitation wavepacket uses a tunneling transistion or it overcomes the barrier thermally assisted [20, 100, 101]. As an alternative, the decay back to its closed state is also possible.
Both the cyclization and the cycloversion occur on the picosecond timescale. An overview over calculations and measurements as well as descriptions for detailed reaction pathways can be found in [20, 102].
Furthermore, for the open isomer of the DCP, two conformations are existing: an antiparallel, photoactive one, which can undergo the open-close reaction and vice versa, and a parallel one, showing no photochromic behaviour [103]. In solution, these two conformations can interconvert freely between each other. The situation is different if the triads are embedded and therefore immobilised, e. g. in a polymer matrix, where only a population which was deposited in its closed or antiparallel open state can undergo switching.
Yet there is still one drawback: molecules from the DCP family themselves show only weak

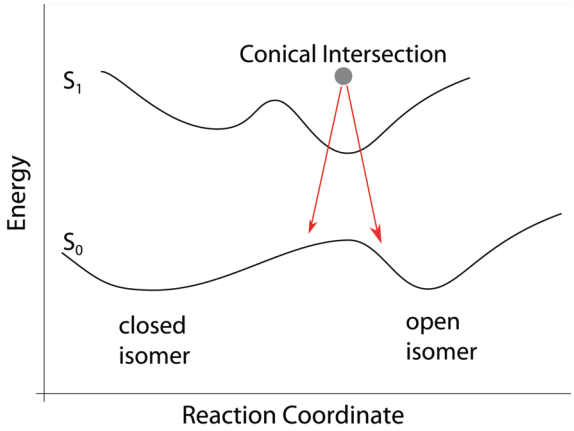

Figure 2.4.: *Strongly simplified energy surfaces of the ground (S_0) state and the first electronically excited (S_1) state of a dithienylcyclopentene molecule. Each potental surface features two minima, one for the closed state of the DCP (left), and one for the open state of the DCP (right), separated by an energy barrier. Upon excitation above the S_1 surface, the photophysical reactions can proceed through conical intersections (Con.In.), of which one is shown. At this conical intersection, relaxation to the ground state can either happen to the open or the closed state of the switch (red arrows). The figure has been adapted from [99].*

fluorescence [20]. One strategy to enhance fluorescence is to introduce functional groups which enlarge the fluorescence quantum yield of the switch itself and - as a by-product- fine-tune spectral properties together with the suitability for different pH regimes, which is highly interesting for super-resolution microscopy applications in the life sciences [15].

3. Molecular Switches and Fluorophores - Photochromic systems

3.1. Photochromic Triads

Another strategy to enhance the fluorescence output makes use of macromolecular chemistry. A concept of combining functional molecules in order to achieve desired characteristics in switching and fluorescence relies on the advantages of each type of molecule [104]. Following this strategy, with the DCP as the molecular switch and strong fluorophores covalently linked as fluorescence markers, photochromic molecules with a high fluorescence quantum yield can be synthesized [21, 61, 105–108] . Figure 3.1 demonstrates the switching process with a fluorophore present, in this case perylene bisimide (PBI) (see Figure 3.1 a)). In the case for the open switch DCP (top), the excitation (e. g. visible light, indicated by the green arrow) cannot be transferred from the PBI to the DCP as its first excited state S_1 lies too high. In order to return to the ground state S_0, the PBI shows fluorescence (orange arrow). In the other case (see Figure 3.1 a), bottom), where the DCP is present in its closed form, the excitation energy can be transferred to the DCP because its excited state is now switched to a level low enough to be reached by the PBI excitation (horizontal dashed arrow) [109, 110]. The DCP returns to the ground state in a radiationless process (vertical dashed arrow). Having a look at the spectrum for the system DCP-PBI, the situation is as follows (Figure 3.1 b)). One can see the absorption spectra for DCP and its closed (blue line) and open (red line) state. As the absorption band in the visible range is only present in the closed state of the DCP, a spectral overlap with the emission spectrum of PBI (orange line) is also only present for the closed state of the DCP. Thus, the quenching of fluorescence only happens for the closed form of the DCP as described above, for the open form, a nearby PBI will show fluorescence [21].

For this dissertation, tree kinds of photochromic triads are important to mention. They all consist of one DCP switch and two strong fluorophore moieties. Measurements and Experiments will be presented in chapters 5 and 6. The triads were synthesized and kindly

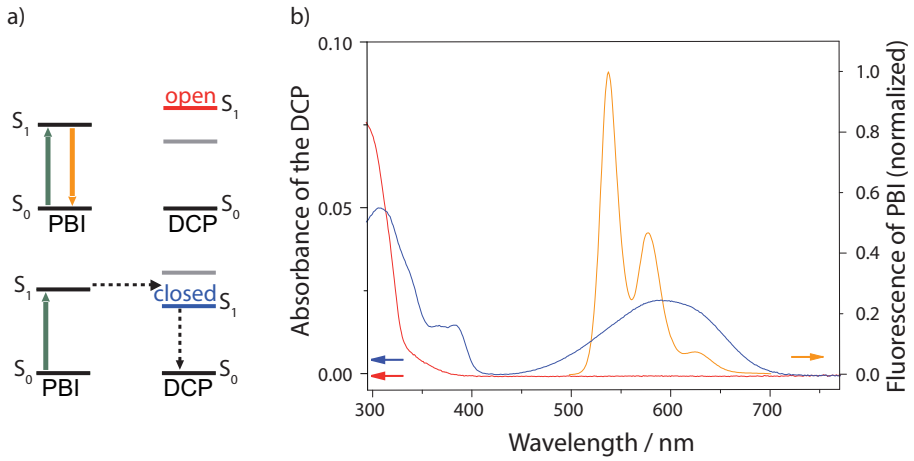

Figure 3.1.: *a) A scheme for the energy transfer process present in triads consisting of a DCP switch and a fluorophore, in this case PBI. In the open state of the triad (top), the S_1 energy level lies too high to be reached by an excitation from the PBI. An excited fluorophore (green arrow) can only return to its ground state S_0 by fluorescence (orange arrow). The situation is different for the closed state of the triad (bottom). The excited PBI can transfer its excitation energy to the closed DCP, because the S_1 state is now switched to a level low enough to be reached by the PBI excitation. The dashed arrows here indicate radiationless processes for energy transfer and return to the ground state of the DCP. b) The absorption spectra of the closed (blue line) and the open (red line) state of the DCP switch, measured in toluene solution. In addition, the fluorescence spectrum of PBI (orange line) is shown which has no overlap with the absorption spectrum of the open DCP, but a clear spectral overlap with absorption spectrum of the closed DCP. Adapted from [69] and [106]*

provided by the workgroup of Prof. Dr. M. Thelakkat in the Macromolecular Chemistry department of the University of Bayreuth.

1. This triad with the full name (1,2-Bis(2- methyl-5-(4-(N-(pentadecan-8-yl)-perylene-3,4:9,10 tetracarboxy-bisimid) benzyl)thiophen- 3-yl)hexafluorocyclopentene) [25] consists of the DCP switch in the center, one phenyl ring on each side and the PBI fluorophores covalently linked on each side, see Figure 3.2. It is used in [21, 22, 65, 66, 69, 111] and presented here as the reference triad for the single-molecule experiments. The synthesis of this photochromic triad is described in the Supporting Information of [21]. It shall be called **Triad 1** hereafter.

2. The triad 1,2-Bis(2-methyl-5-(N-(pentadecane-8-yl)-perylene-3,4:9,10-tetracarboxy-bisimid)-1,1-biphenyl)thiophen-3-yl)hexafluorocyclopentene) is used in Chapters 5 and 6 and differs from the above-mentioned triad slightly. Instead of having only one phenyl ring in between the DCP switch and the PBI fluorophores, it features a larger distance between the building blocks with a second phenyl ring, see Figure 3.3. For the synthesis of this triad, see the Supporting Information of [106]. This

Figure 3.2.: *The photochromic triad (1,2-Bis(2- methyl-5-(4-(N-(pentadecan-8-yl)-perylene-3,4:9,10 tetracarboxy-bisimid) benzyl)thiophen- 3-yl)hexafluorocyclopentene). It shall be call **Triad 1** hereafter and consists of the photochromic dithienylcyclopente (DCP) switch in the center and two perylene bisimide (PBI) fluorophore molecules covalently linked via one phenyl bridge.*

triad shall be called **Triad 2** hereafter.

Figure 3.3.: *The triad 1,2-Bis(2-methyl-5-(N-(pentadecane-8-yl)-perylene-3,4:9,10-tetracarboxy-bisimid)-1,1-biphenyl)thiophen-3-yl)hexafluorocyclopentene) consists of the DCP switch and two PBI moieties whicht are covalently linked via a bisphenyl bridge. It shall be called **Triad 2***

3. The third triad used is called 1,2-Bis(2-methyl-5-)(4-(1,3,5,7-tetramethyl-2,6-diethyl-4,4-difluoro-4-bora-3a,4a-diaza-s-indacence)1H-1,2,3-triazol-4-yl)benzyl)thiophen-3-yl)hexafluorocyclopentene) and uses boron dipyrromethene (BODIPY) fluorophores, see Figure 3.4. It is used for experiments in chapter 6. This triad will be called **Triad 3**.

Figure 3.4.: *The third triad used (called **Triad 3** hereafter) is substituted with boron dipyrromethene (BODIPY) fluorophores. Its official name is 1,2-Bis(2-methyl-5-)(4-(1,3,5,7-tetramethyl-2,6-diethyl-4,4-difluoro-4-bora-3a,4a-diaza-s-indacence)1H-1,2,3-triazol-4-yl)benzyl)thiophen-3-yl)hexafluorocyclopentene).*

PBI and BODIPY are both well-known fluorophores [112–117], contributing to the triads with a high fluorescence quantum yield and thus, a bright fluorescence signal.

3.2. Experiments with Photochromic Triads

In two publications [21, 22], the fluorescence of an ensemble of **Triad 1** ($1.4 \cdot 10^{-5} moll^{-1}$ triads in a sample with a thickness of about 10 μm, see [21, 22])) was examined as the function of two conversion beams. Beams with wavelengths of 300 nm and 635 nm served for the cyclization and the cycloreversion reaction, respectively. The fluorescence was probed with a wavelength of 514 nm. As the major result of this publication, Pärs et al. have demonstrated the two main characteristics of a transistor, which is in this case operated with photons instead of electrons. First, the gating is demonstrated by being able to switch the ensemble of triads between a highly fluorescent "On"-state and an "Off"-state showing clearly reduced fluorescence. Depending on the intensity of the conversion beams, a modulation ratio of 0.73 [21] or up to 0.8 [22] could be achieved here, values which are well suited for the discrimination between the two states. Second, the amplification feature of a transistor was shown. By calculating the numbers of photons needed for the photochromic reactions [21], which amount to about 10 UV photons for the cyclization process, and about 100 photons (cycloreversion with 514 nm) or several thousand photons (cycloreversion with 635 nm) it was demonstrated that relatively small numbers of photons can control the flow of tens or hundreds of millions of fluorescence photons from the PBI moieties of the triad. By the way it was found that due to a remaining crosstalk in the system, already two wavelengths, 300 nm and 514 nm, are sufficient to convert between the two states. From these two studies, which are aiming at applications in molecular electronics, the question arises whether single photochromic molecules can be exploited as single transistors, the climax in miniaturization.

In a subsequent publication [25], the focus of the study was directed to the achievable contrast for a modulation experiment where the triads were continuously probed with visible light (514 nm) and periodically brought to low fluorescence by additionally applying UV light (514 nm). With both wavelengths illuminating the sample, a competing process of cyclization and cycloreversion takes place, resulting in a steady-state of fluorescence at a low level. In other words, the achievable contrast ratio $1/C$ depends linearly the ratio of the two light intensities I_{300} and I_{514},

$$\frac{1}{C(I_{300}, I_{514})} \sim \frac{I_{514}}{I_{300}}. \tag{3.1}$$

The detailed derivation for the achievable contrast ratio is given in [25], providing a powerful tool for the setting of the illumination intensities when experiments with high contrast between the two states are carried out and gives valuable information when the experimental interest changes to single molecule experiments.

3.3. Fluorescence of Single Molecules and the Presence of Blinking

Because this dissertation deals with the digital switching of single molecules between a bright and a dark state, one has to be careful with the fact that single molecules or, more generally speaking, single nano-objects, undergo reversible, stochastic transitions between bright and dark states in their fluorescence, summarized under the term "blinking" [62, 63, 118, 119] and shall be discussed here briefly.
Blinking, i. e. the distribution of times a single nano object remains in a dark or bright state, covers essentially all experimentally accessible time scales, and is described mathematically by a power-law relation

$$P(\tau) \sim \tau^{-\alpha} \tag{3.2}$$

for the distribution P of the bright and dark states, with the power-law exponent α [62].
It can be described by processes a nano-object faces in its electronically excited state. Upon excitation, a photoionization can occur, and a charge separation to the environment of the molecule may take place. In an ideal environment, depicted by a smooth energy landscape around the single fluorescence emitter, the charge recombination could be easily achieved as the separated charge can just relax to the minimum of the potential well. However, in real environments, the energy landscape around a single emitter is not smooth, but shows local minima in which a separated charge can be trapped. In order to leave such a trap state, e. g. tunneling processes need to be run through in order to achieve recombination at the single emitter site in the energy landscape [62].
To summarize, when trying to access the switching of single photochromic molecules, blinking has to be taken into consideration, too, as the two processes "switching" and "blinking" both lead to the same result - a dark state of no fluorescence.

3.4. Experiments with Single Photochromic Molecules

In 2002, Irie et al. reported the switching of single photochromic molecules consisting of a DCP switch and and anthracene moiety as the fluorophore [58], which was studied by confocal microscopy. These dyads (one switch - one dye molecule) were prepared in a polymer film in their closed, non-fluorescent state. Upon illumination with visible light for 10 s, triads which had switched to the fluorescent state could be identified in the sample. By applying UV light for another 3 s, the fluorescence ceased and reappeared upon another 10 s period of visible illumination. In another setting of the experiment the molecule was illuminated continuously with both visible light (488 nm, $200 W/cm^2$)

and UV light (325 nm, $0.027 mW/cm^2$) and the fluorescence was recorded with an APD sampled with a dwell time of 20 ms in order to average out short-term blinking, yielding a distribution of times single photochromic molecules stayed in the "On"-state, with an accumulation of the "On"-times around 10 s [58]. However, the influence of long-term blinking which happens at timescales accessible by the 20 ms dwell time, is left uncertain. Similar findings were presented in another publication by Fukaminato et al. [59], where the single-molecule switching for two slightly different molecules of the DCP-anthracene type (as mentioned above) was monitored both in fluorescence imaging and confocal microscopy. Concerning fluorescence imaging, image frames are presented which show bright spots as the single-molecule fluorescence after visible illumination (5 s), and the disappearing of those spots in frames after UV illumination (again, 5 s). However, also frames can be found where some of the molecules remain in their dark state upon visible illumination for at least 5 s and start to show fluorescence only after a 10 s visible illumination. In the publication this fact is assigned to different response times for different triads [59]. Again, another possible explanation is the presence of a long-term blinking event causing a dark state. Concerning confocal microscopy, single molecules are illuminated with both visible and UV light, and fluorescence intensity traces recorded with a binned time of 20 ms are shown, with alternating "On"- and "Off"-states, of which 1-3 were collected per molecule. The "On"-times were recorded for a fixed visible illumination intensity (488 nm, $100 W/cm^2$) and three different UV intensities (325 nm, $0.027 mW/cm^2$, $0.054 mW/cm^2$, and $0.27 mW/cm^2$, featuring a decrease in the average "On"-time (11 s, 5.7 s, and 1.2 s, respectively). Vice versa, the dependence of the "Off"-time on the visible illumination (488 nm, $50 W/cm^2$, $100 W/cm^2$, and $300 W/cm^2$) for a fixed UV illumination intensity (325 nm, $0.054 mW/cm^2$) was examined. Here the average "On"-time shows a decrease upon increasing the visible illumination intensity, from 23 s over 11 s to 4.0 s. This change is assigned to the photochromic switching of the molecules. To confirm that this dependence is indeed due to photoswitching, Fukaminato et al. repeated the experiment with a fixed visible illumination intensity and three different UV intensities for the slightly different substituted molecule with a significantly higher cycloreversion quantum yield (20-50 times) , leading to significantly shorter average "Off"-times (220 ms) [59].
A molecule composed of DCP and a PBI derivate then led to the publication of [61] with a similar setup as [59]. Again, the distribution of "Off"-times was examined and it was found that it decreased with decreasing UV intensity. In addition to that, the dependence of the "Off"-times of the polymer matrix the molecules were embedded in was studied and the results were assigned to the glass transition temperatures (T_g), and therefore the rigidity of the matrix at room temperature conditions, culminating in the claim that for the polymers with high T_g, the photochromic reaction is mechanically hindered, resulting in

both longer average "On"- and "Off"-times, compared to the measurements with one low T_g matrix [61]. However, due to the different (local) environments of the single molecules represented by the different polymer materials, this could also be assigned to different blinking characteristics.
In a fourth publication, Fukaminato et al. report on the non-destructive fluorescence readout of a single dyad consisting of a DCP switch and a PBI fluorophore [60]. The molecule was designed and synthesized in such a way that the absorption spectrum of the DCP both in its open and closed state does not overlap with the emission spectrum of the PBI, thus preventing energy transfer from the PBI to the DCP. As a consequence, the state of the switch can be accessed with UV (330 nm to 380 nm, "erasing") and visible light (440 nm to 490 nm, "writing") and not by the third wavelength (532 nm) used for probing. The quenching of fluorescence takes place in the open state of the switch induced by the visible wavelength. This is, for the photochromic system studied here, due to an intramolecular electron transfer process [60].

3.5. Considerations for the Design of Experiments on Single Photochromic Triads

The key consideration when designing experiments dealing with single molecule fluorescence is the fact that due to the rather low number of photons a single molecule emits compared to ensembles of fluorophores, the experimentalist is confronted with the challenge to detect as many of those photons as possible. This fact becomes even more prominent when the molecules can convert between a bright and a dark state, and these states need to be discriminated from each other distinctively.
In [69], I have made an estimation for the count-rate, i. e. the rate of photons registered by a detector during a certain sampled time, to be in the range of $\approx 10 cts/s$, or roughly calculated, $0.1 cts/10 ms$ if the detector is sampled with a bin time of 10 ms, given that a single **Triad 1** is excited to fluorescence with an intensity of $I_{488} = 1 W/cm^2$. Unfortunately, one already has to assume a dark count rate of the detector of $1 cts/10 ms$, leading to the conclusion that the excitation intensity needs to be increased in order to increase the fluorescence output of the single triad. However, increasing the visible illumination leads to a faster cycloreversion reaction, as the rate k_{co} is directly proportional to the probe beam intensity [25], thereby shifting the ring-opening reaction to shorter time scales. So, in order to step out of this dilemma, a strategy to slow down the ring-opening reaction is favoured, together with a high count-rate for the fluorescence.
A slowing of the cycloreversion reaction was implemented in two ways. First, **Triad 2** was synthesized by the workgroup of Prof. Dr. Mukundan Thelakkat, with a second phenyl

ring between DCP and PBI with respect to **Triad 1**, enhancing the distance between the two functional moieties of the triad. This enhancement of the distance goes along with a reduced energy transfer efficiency from the donor PBI to the acceptor DCP, as energy transfer depends strongly on the distance between donor and acceptor [109, 110] and a reduced energy transfer efficiency will therefore result in a reduced cycloreversion reaction, with the assumption that the energy transferred from the PBI is responsible for the cycloreversion reaction. Second, the cycloreversion reaction features a thermal component [101, 120]. This feature was shown for the fluorescence of **Triad 1** in [65] and led to the publication of [66]. Briefly, the ring-opening reaction is slowed down to 0.7% with respect to its room temperature value. More precisely, the ring-opening (cycloreversion) quantum yield is reduced from its room temperature value of $\varphi_{co} = 4.43 \cdot 10^{-3}$ to $\varphi_{co} = (2.9 \pm 2.6) \cdot 10^{-5}$ for the low temperature range between 5 K and 150 K [66]. This is why the single molecule measurements presented in this dissertation are all carried out at a fixed temperature of 10 K.

3.6. Theoretical Models

Here, at first a kinetic model for the switching of ensembles of triads is given as an overview and in order to illustrate the contrast to single-molecule experiments described subsequently.

3.6.1. Fluorescence Switching of Ensembles

In this section, the switching of ensembles of triads is discussed and the kinetic model presented [121, 122].
It follows closely the derivations in [25] and [66].
For ensembles of triads, N_t denotes the total number of triads,

$$N_t = N_o + N_c, \tag{3.3}$$

which is the sum of triads in the open N_o and in the closed N_c state, respectively. The triads interconvert between the two states by illumination with light of the appropriate wavelength, see Figure 3.5. The cyclization reaction (open $\rightarrow$ close) and the cycloreversion

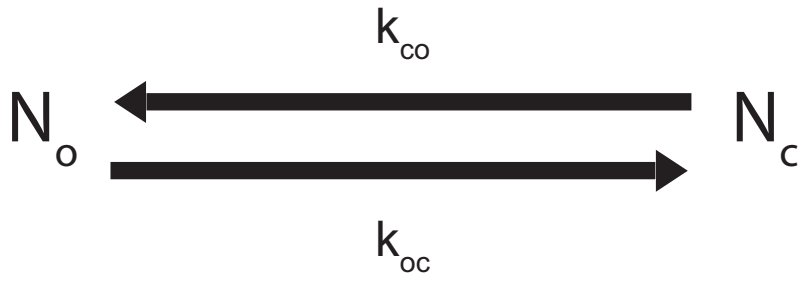

Figure 3.5.: *Schematic Reaction Used for Triads Switching between open N_o and closed N_c populations with the rates k_{oc} and k_{co} for the reverse reaction.*

reaction (close $\rightarrow$ open) can be described by the rates

$$k_{oc} = \frac{I_{325}}{h\nu_{325}} \cdot \sigma_{325} \cdot \varphi_{325} \text{ for the open } \rightarrow \text{ close reaction} \tag{3.4}$$

and

$$k_{co} = \frac{I_{488}}{h\nu_{488}} \cdot \sigma_{488} \cdot \varphi_{488} \text{ for the close } \rightarrow \text{ open reaction.} \tag{3.5}$$

Here, I_{325} and I_{488} denote the illumination intensities at 325 nm and 488 nm, respectively, divided by the photon energies $h\nu$ at the respective wavelengths. Briefly, the fractions in the front of the Equations 3.4 and 3.5 refer to a photon current hitting the sample, which absorbs the photons according to the absorption cross sections $\sigma_{325/488}$ and will switch to the corresponding state with the switching quantum yield $\varphi_{325/488}$.

The decay of fluorescence upon UV illumination

In a typical experiment for ensembles, the triads are initalized in the open state by illumination with visible light, i. e. $N_o(t=0) = N_t$. If the sample is now illuminated with UV light additionally, the number of open triads changes, following a rate equation illustrated by Figure 3.6:

$$\frac{dN_o}{dt} = \dot{N}_o = -k_{oc}N_o + k_{co}N_c \tag{3.6}$$

For this simple differential equation, the specific solution yields

$$N_o(t) = N_t \left(\frac{k_{oc}}{k_{oc}+k_{co}} \cdot e^{-(k_{oc}+k_{co})t} + \frac{k_{co}}{k_{oc}+k_{co}} \right) \tag{3.7}$$

and

$$N_c(t) = N_t - N_o(t) = N_t \left(1 - \left(\frac{k_{oc}}{k_{oc}+k_{co}} \cdot e^{-(k_{oc}+k_{co})t} + \frac{k_{co}}{k_{co}+k_{oc}} \right) \right) \tag{3.8}$$

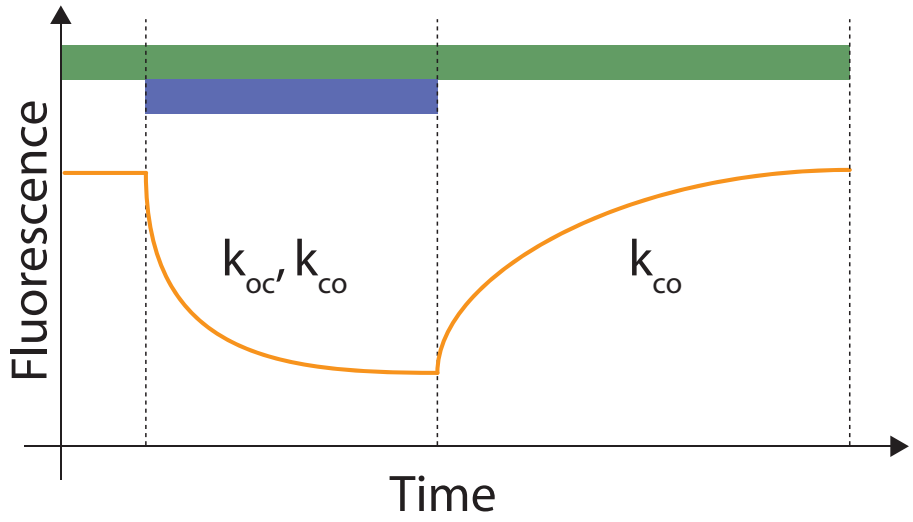

Figure 3.6.: *A typical modulation experiment for triads switching between open N_o and closed N_c populations. The green and the blue bar on top indicate the illumination sequence with the intensities I_{488} (green bar) and I_{325} (blue bar), respectively. The orange line illustrates the fluorescence, which is proportional to N_o. In the beginning, the fluorescence signal is constant, as only visible light excites the molecules. Upon additional illumination with UV light, a competing process of cyclization and cycloreversion reactions begins, where the rates k_{oc} for the open-to-closed and k_{co} for the close-to-open reaction are assigned. In the signal, this can be seen in a reduction of fluorescence. After the UV illumination is ceased again, the triads convert back to the open state, and fluorescence recovers with the rate k_{co}.*

In the next step, the fluorescence is connected to the number of triads in the open and closed state via

$$\begin{aligned}
F(t) &= C\cdot\left(\Phi_f^o\cdot N_o(t)+\Phi_f^c\cdot N_c(t)\right)\\
&= C\cdot N_t\left((\Phi_F^o-\Phi_F^c)\left(\frac{k_{oc}}{k_{oc}+k_{co}}\cdot e^{-(k_{oc}+k_{co})t}+\frac{k_{co}}{k_{oc}+k_{co}}\right)+\Phi_F^c\right)\\
&= \underbrace{C\cdot N_t\cdot\Phi_F^c+C\cdot N_t\cdot(\Phi_F^o-\Phi_F^c)\cdot\frac{k_{co}}{k_{oc}+k_{co}}}_{B}\\
&+ \underbrace{C\cdot N_t(\Phi_F^o-\Phi_F^c)\cdot\frac{k_{oc}}{k_{oc}+k_{co}}}_{A}\cdot\underbrace{e^{-(k_{oc}+k_{co})t}}_{\exp-\lambda t}\\
&= B+A\cdot e^{-\lambda t} \qquad (3.9)\\
\text{with } \lambda &= k_{oc}+k_{co}.
\end{aligned}$$

with the fluorescence quantum yields Φ_f^o and Φ_f^c for the open and closed state of the triad, respectively. Furthermore, the constant C is introduced here. This constant contains factors dealing with experimental and molecular characteristics, i. e. absorption cross section,

excitation intensity, quantum efficiency of the detector and the light collection efficency of the setup.
Following this illumination, the fluorescence will reach a steady state, as the two illumination intensities I_{325} and I_{488} balance the reaction so that $\frac{dN_o}{dt} = 0$ (see Equation 3.6). Setting Equation 3.6 into 3.3 one yields this steady state

$$N_o(t) = N_t \cdot \frac{k_{co}}{k_{co} + k_{oc}}, \tag{3.10}$$

which is, at the same time, the initial condition for the cycloreversion reaction.

The return of fluorescence under visible illumination

For a modulation experiment, the cycloreversion reaction is the return of fluorescence from the steady state to the high state when the UV illumination is ceased. Equation 3.6 now yields the specific solution

$$N_o(t) = N_t \left(1 - \frac{k_{oc}}{k_{oc} + k_{co}} \cdot e^{-k_{co}t}\right) \tag{3.11}$$

and

$$N_c(t) = N_t \frac{k_{oc}}{k_{oc} + k_{co}} \cdot e^{-k_{co}t}. \tag{3.12}$$

Again, these numbers can be connected to the fluorescence of the sample and one yields

$$\begin{aligned} F(t) &= \underbrace{C \cdot N_t \Phi_F^o}_{B} + \underbrace{C \cdot N_t \cdot (\Phi_F^c - \Phi_F^o) \cdot \frac{k_{oc}}{k_{oc} + k_{co}}}_{A} \cdot \underbrace{\exp -k_{co}t}_{e^{-\lambda t}} \\ &= B + A \cdot \exp -\lambda t \end{aligned} \tag{3.13}$$

with

$$\lambda = k_{co}$$

Summarizing, both the ring-closure and the ring-opening reaction of an ensemble of triads can be described by an exponential decay and an exponential growth, respectively.

3.6.2. Fluorescence Switching of Single Photochromic Triads

In this section, expectations for an experiment probing the switching of single photochromic triads are formulated. The section follows [123] and [69].
For the experiments on single photochromic triads, the situation is different from the one for ensembles of triads. As there is only one fluorescent photochromic molecule, one cannot observe the switching as exponential decay or saturated exponential growth for the

cyclization and cycloreversion reaction, respectively. The expectation for the fluorescence switching of single triads is a digital “Off”- to “On”-switchting between the closed, non- or weakly fluorescent form of the triad and the open, fluorescent one and vice versa. However, triads suffer from one inherent drawback on intentional switching which is the crosstalk between readout and the “On-”reaction. To be more precise, the crosstalk leads to a re-opening of the triads when probing the state of the switch with visible light, going along with a return of fluorescence.

Yet, one can also make use of the crosstalk by designing experiments which probe the

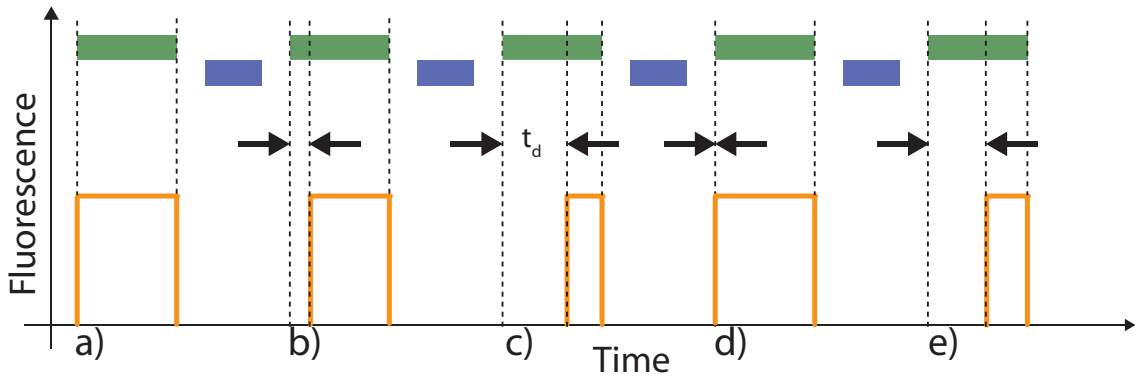

Figure 3.7.: *An experiment for probing single photochromic triads. Here, alternating illumination with visible light (*488 nm*, green bars) and UV light (*325 nm*, blue bars) is used to examine the switching of single triads. a) in this first cycle, a triad shows fluorescence starting with the onset of illumination. b), c) and e) as a cyclization due to UV illumination has taken place before probe illumination with visible light, the onset of fluorescence is delayed with respect to the onset of green illumination. This is due to the fact that the triad has changed to the dark, closed state upon UV illumination and recovers back to the open state, due to the stochastic nature of the intramolecular processes with a statistically distributed delay time t_d. The different times are marked with the black arrows. d) This delay time can be too short for detection or no switching to the closed state has taken place, and so also delay times ”0” are present.*

so-called “destructive readout” of the fluorescence (see Figure 3.7). If single triads are initialised in their closed, non-fluorescent state (blue bar), they will cycle in this state with energy transfer from the fluorophore to the switch for a statistically distributed time (thick black arrows). This time t_d is visible as a delay in the onset of fluorescence (orange) with respect to the probe laser illumination (green bars). For the repetition of those illumination sequences, different delay times are expected to occur (indicated in Figure 3.7 b) to e)). If the pre-initialisation with UV light is not present (see Figure 3.7 a)), the fluorescence is expected to promptly start with visible light illumination. The key consideration behind the sequential illumination experiment is the stochastic nature of photon absorption in the triads and the so-called Poisson-process and its inter-arrival-time distribution [123], which will be presented here.

Poisson Process

A process is called a Poisson-process with the rate $\lambda > 0$, if a counting process $\{N(t), t \geq 0\}$ features the following characteristics:

(i) $N(t=0) = 0$, i. e. the counting process begins at "0".

(ii) The process contains independent increments. If the number of counting events in different counting intervals are independent of one another, this condition is fulfilled.

(iii) The number of events in one counting interval of the length t follows a Poisson distribution with the mean λt, accounting for all times t with $t \geq 0$:

$$P\{N(t+s) - N(s) = n\} = e^{-\lambda t} \cdot \frac{(\lambda t)^n}{n!}, \quad n = 0, 1, \ldots \tag{3.14}$$

Inter-arrival-time distribution for the Poisson Process

The basis for the inter-arrival-time distribution is the aforementioned Poisson process. Here, the focus is on the time X_n between the $(n-1)$th and the nth event. The sequence $\{X_n,\ n \geq 1\}$ is then called the sequence of inter-arrival times, from where the distribution of inter-arrival times X_n can be derived.
The first event $\{X_1 > t\}$ only takes place if no other event has occured in the interval $[0, t]$. Accordingly, $N(t) = n = 0$ is set into Equation. 3.14, yielding

$$P\{X_1 > t\} = P\{N(t) = 0\} = e^{-\lambda t}. \tag{3.15}$$

This is an exponential distribution for X_1 with a mean $1/\lambda$. Having a process with no memory, this exponential distribution also accounts for all following time spans X_n, as the experiment can be seen as newly started after every single event.
Now, the probability density, which describes the arrival times for all n, is of interest,

$$P\{N(t) \geq n\} = \sum_{j=n}^{\infty} e^{-\lambda t} \cdot \frac{(\lambda t)^j}{j!}. \tag{3.16}$$

Then, the inter-arrival time distribution is derived as the probability density function of Equation. 3.16 by differentiation:

$$f(t) = \lambda \cdot e^{-\lambda t} \cdot \frac{(\lambda t)^{n-1}}{(n-1)!} \overset{n=1}{=} \lambda \cdot e^{-\lambda t}. \tag{3.17}$$

Here, $n = 1$ is set so that one yields the arrival time distribution only for the first event [123].

The transition to a single molecule experiment

First, the absorption process is assigned to Poissonian statistics.
The absorption of Photons by single molecules is also given by a rate,

$$k_{abs} = \sigma_{488} \frac{I_{488}}{E_{488}}, \tag{3.18}$$

where σ_{488} is again the absorption cross-section for photons of 488 nm wavelength, and the fraction of the intensity I_{488} and the photon energy E_{488} the photon current hitting a molecule.
The absorption cross-section is a measure for the probability to absorb one photon, and this probability is low, $\sigma_{488} = 8.328 \cdot 10^{-17} cm^2$ for **Triad 1** (calculated according to [21]). Together with the only two possible outcomes absorption - no absorption, this fulfills two requirements of Poissonian statistics. The third one, a high number of trials of this probabilistic experiment, is delivered by the photon current which amounts to $\approx 10^{18} photons/(s \cdot cm^2)$. for an illumination intensity of $1W/cm^2$
This Poissonian nature will also be found in the ring-opening reaction, as the absorption rate k_{abs} from Equation 3.18 can be found in the ring-opening rate (equation 3.5)

$$k_{co} = \varphi_{co} \sigma_{488} \frac{I_{488}}{E_{488}}$$

where φ_{co} denotes the quantum yield for the ring-opening reaction. With this finding, equation 3.17 transforms to

$$f(t) = k_{co} \cdot e^{-k_{co} t} = \frac{1}{\tau_{On}} \cdot e^{-\frac{t}{\tau_{On}}}, \tag{3.19}$$

the waiting time distribution for the first event (fluorescence jumps to the “On”-state). Here, τ_{On} is introduced as the inverse of k_{co}. It is the average time of the decaying exponential distribution, or briefly, the average time a single triad remains in the closed state under probe illumination, before it undergoes the photocycloreversion reaction and the fluorescent state is reached again.

4. Experimental Setup and Sample Preparation

4.1. The solid immersion objective

Microscopy at low temperatures involves on the one hand advantages concerning the stability of the sample and the fact that the switching event of single photochromic triads is slowed down [65, 66]. On the other hand, the collection of as many photons as possible is crucial for single-molecule fluorescence microscopy. Therefore, the improvement of the resolution, accompanied by the collection efficency the of optics, is the key strategy to increase the fluorescence signal detected from the sample. A measure for these characteristics is the numerical aperture numerical aperture (NA) of an objective [124],

$$NA = n \cdot \sin(\Phi). \tag{4.1}$$

Here, n denotes the refractive index of the medium between objective and sample, and Φ is the so-called acceptance angle of the objective. The advantage of enhancing the NA becomes obvious with a look at the collection efficiency I [125],

$$I \sim NA^2, \tag{4.2}$$

depending on the square of the NA. As a consequence, one can improve two parameters in order to improve the NA of an optical system. First, the acceptance angle can be increased by the construction of appropriate optics, yet it is limited to a theoretical maximum angle of 90° [124]. Second, the refractive index n between objective and sample can be enhanced, which leads to the concept of immersion.

Immersion with liquids

Figure 4.1 illustrates different objective setups. In Figure 4.1 a), the space between the objective and a glass cover slip on the sample is filled with air. Here, the collection of

a fluorescence signal from the sample is hindered due to the different refractive indices of glass and air, leading to the effect that light is refracted away from the objective, or never even reaches it as total internal reflection prevents it from leaving the glass in the direction of the objective. The refractive index mismatch can be eliminated (partially) by the introduction of an immersion liquid (oil or water) with a refractive index close or equal to that of the cover slip, see Figure 4.1 b). In this way, the NA can be improved because rays that would have been lost for collection in an air setup, can still be recorded. Such highly optimized systems can feature an NA of 1.3 - 1.4 [124, 126].

However, when measuring at low temperatures, liquid immersion media are not practical,

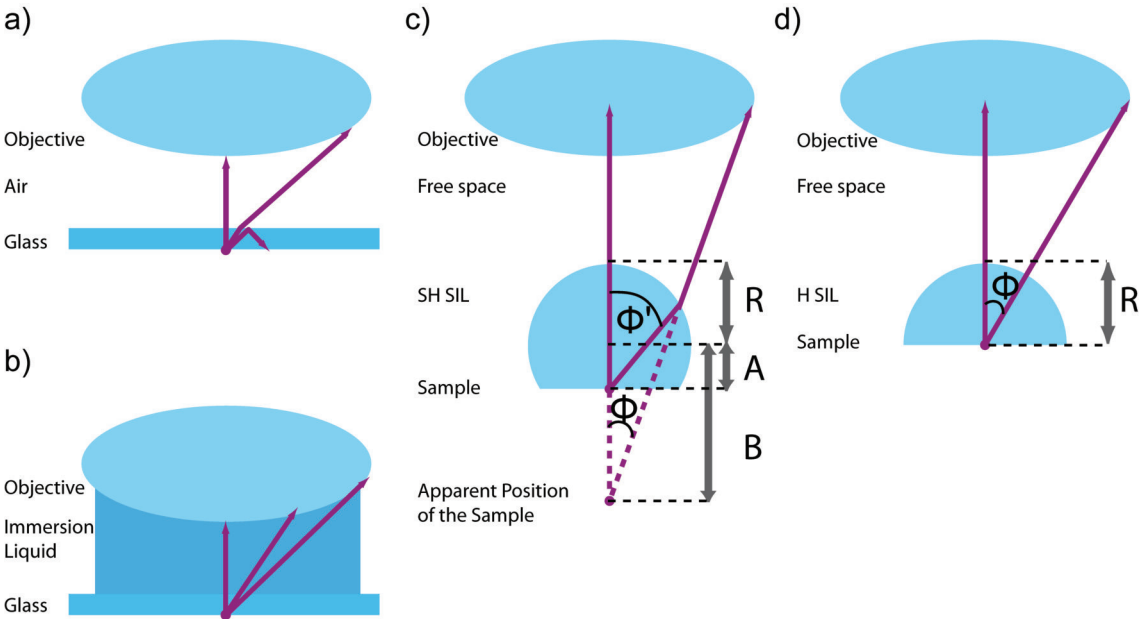

Figure 4.1.: *Various Optical Setups for the collection of fluorescence signals. a) A setup where the fluorescence is collected through a glass cover slip, with an air distance between objective and cover slip. Due to the step in the refractive index on the border glass-air, light is either refracted away from the objective or total internal reflection occurs which is suppressed partially or completely in b), where a specially designed objective and an immersion liquid is applied. c) A solid immersion setup consisting of an objective and a superhemispheric solid immersion lens (SH SIL). It is a sphere, flattened on the bottom, described by the Radius R and a thickness parameter A. The application of the SH SIL concept increases the acceptance angle to Φ' compared to the situation of the objective without SH SIL, and the respective acceptance angle Φ. The apparent position of the sample is then located at a distance B from the center of the sphere. d) The concept for a hemispheric SIL (H SIL). This half sphere with a radius R also increases the NA, as it suppresses total internal reflection due to the fact that rays collected from the sample leave the SIL perpendicular to its surface. Figure adapted from [68]*

due to the freezing of the immersion liquids [127]. This would make it impossible to adjust the focus or scan laterally on the sample. Another drawback is the lack of the ability to measure under oxygen-free conditions, as a vacuum pump would also remove the immersion liquid from the sample chamber. Because of this, the concept of solid

immersion [67] was introduced.

Solid Immersion

Having a look at Equation 4.1, microscopy at low temperatures would be limited to "1" because the theoretical maximum acceptance angle Φ is limited to 90°, and the refractive index of vacuum is also equal to "1" (or at least close to that value with a remaining atmosphere).
Nevertheless, a way to enhance the NA is the application of a solid immersion lens (SIL)[67, 125, 128–131], which is the smart design of the back of a cover slip [68]. Figure 4.1 illustrates objective setups with a superhemispheric SIL (SH SIL) (Figure 4.1 c)) and and a hemispheric SIL (H SIL) (Figure 4.1 d)). The superhemispheric SIL is a sphere with a radius R, which is flattened so that its total thickness can be described by R and the so-called thickness parameter A, denoting the distance from the flattened side to the original center of the sphere. An additional focussing of the rays is achieved by the curved surface of the SIL, leading to an increase of the acceptance angle from Φ to Φ' with respect to the situation without SIL. The apparent position of the sample is then shifted to a distance B from the center of the sphere. However, commercially availalabe SILs are half spheres, which can serve as hemispheric SILs. Here, the acceptance angle is not enhanced, but total internal reflection is suppressed because the rays can leave the material of the SIL perpendicular to its surface.
In a diploma thesis [68], detailed derivations for the magnification and the NA have been made, of which the two key results will be presented here. The magnification M of a SIL system is calculated as

$$M_{SIL} = \frac{n_{SIL}}{\frac{A}{R}(1 - n_{SIL}) + 1}, \tag{4.3}$$

leading to $M_{HSIL} = n_{SIL}$ for the hemispheric case ($A = 0$) and $M_{SHSIL} = n_{SIL}^2$ for the aberration-free superhemispheric case ($A = R/n$)) with the resulting overall NA of the system objective-SIL $NA_{HSIL} = n_{SIL} \cdot NA_{objective}$ and $NA_{SHSIL} = n_{SIL}^2 \cdot NA_{objective}$, respectively [68]. Again taking into account advantage of improving the collection efficiency (Equation 4.2), both concepts presented here feature benefits [67, 125, 128, 129].
In the following subsection, the application of the SIL for the experiments described later is presented

The application of the SIL in the Sample Holder

The sample holder is a home-built replica of the original ”cold finger” (CF) provided by the cryostat manufacturer *CryoVac*, but remodeled for the use with a SIL [69]. It was fabricated in the mechanical workshop at the University of Bayreuth, see Figure 4.2. The main difference to the original sample holder is the capability to install the SIL on the sample by means of a clamping ring (CR).

The sample holder features a drilled hole in its centre, which is due to the fact that the

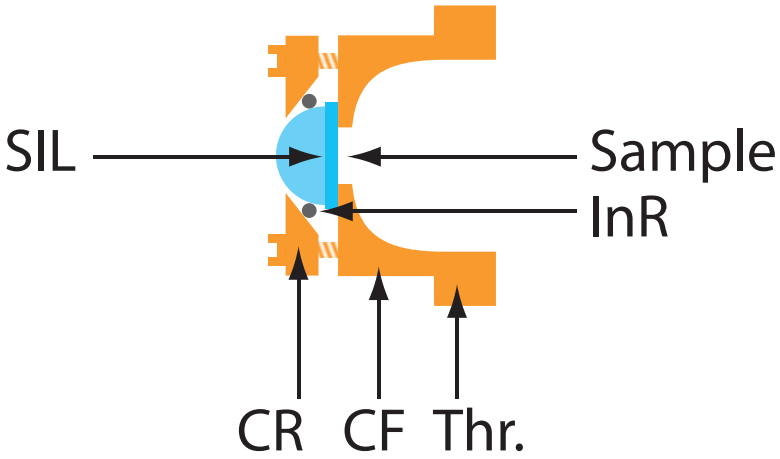

Figure 4.2.: *The sample holder, also called ”cold finger” (CF), which can be screwed into the inner heat exchanger of the cryostat. The solid immersion lens (SIL) is clamped to the back of the sample with a clamping ring (CR) and an indium ring (InR) as a spacer. The threading (Thr.) is located on the right-hand part of the Figure. The Figure was adapted from [69]*

UV laser beam enters the cryostat from the back window, whereas the green (488 nm) beam is focused through the front window of the cryostat with a long-working-distance microscope objective (*Edmund Optics*). The beam is then further focused through the SIL (fused silica half sphere, n = 1.52, *Edmund Optics*) which is centered over the sample with a brass ring (CR, clamping ring). This ring is fixed to the lower part of the sample holder with three screws. As a spacer, an indium ring (InR) is placed between the brass and the SIL, which is pressed to the sample (a rubber ring, for example, would not be suited for low temperature applications). The sample itself is spincoated (see Section 4.4 later on) to a microscope cover slip (thickness range 0.13 mm to 0.16 mm) and faces away from the SIL, as the emission dipoles favour higher refractive index materials [128, 132]. In my master thesis [69], I have shown that the collection efficiency rises by a factor of 1.8 ± 0.1 when applying the SIL. This beneficial factor can help to improve the detection of the single-molecule fluorescence signal.

4.2. Fluorescence Microscope

In order to perform measurements on photochromic fluorescent molecules, a home-built fluorescence microscope was used. With this microscopic setup, one makes use of the characteristic fluorescence emission of the sample itself. [124]

Figure 4.3 illustrates the microscope setup. For the illumination of the sample, two

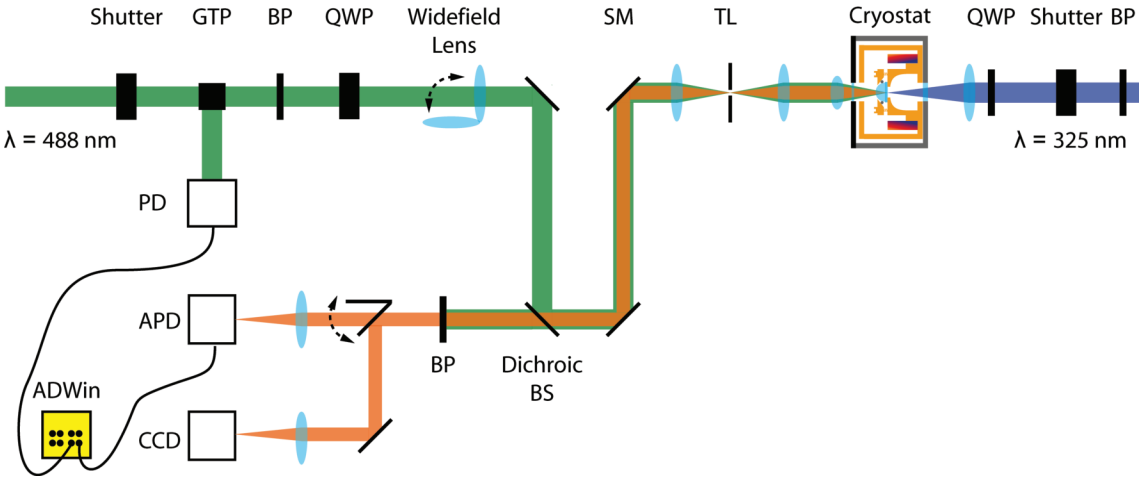

Figure 4.3.: *The Experimental setup for the switching experiments with selected optical components. The probe beam with its wavelength of* 488 nm *is transferred to the setup and first vertically polarized with a Glan-Taylor-Prism (GTP). The horizontal polarization serves as a temporal reference and is recorded with a photodiode (PD). The beam is the spectrally cleaned up with a bandpass (BP) filter and converted to circularly polarized light with a Berek compensator, which is adjusted as quarter wave plate (QWP). After passing a dichroic beam splitter (BS), the sample can be scanned with a scanning mirror (SM) whose pivotal point is imaged to the back aperture of the microscope objective by a telecentric lens system (TL) and is focussed through the front window and the solid immersion lens (SIL) to the sample. The fluorescence is collected by the same objective system and transmitted through the BS on its way back. Another bandpass (BP) removes residual stray light from the fluorescence signal. The signal is recorded either with an avalanche photo diode (APD) in confocal mode, or, with the mirror and widefield lens flipped into the beam path, with a CCD camera (CCD). The UV conversion beam is also spectrally cleaned up by a bandpass (BP) filter, and its linear polarization is converted to circular polarization with a quarter wave plate (QWP) before the beam is focussed to the sample through the back window of the cryostat with a lens. The timing of the illuminations is achieved by electromechanical shutters, which are controlled by an ADWin measurement processor. This processor also records the data from PD and APD.*

different wavelengths need to be coupled into the microscope setup.

The UV beam with a wavelength of 325 nm is generated in a helium-cadmium laser (HeCd-Laser, see Table A.2) and causes the ring-closure reaction of the photochromic triads. Its intensity can be adjusted with a variable optical density (OD) wheel right after the laser beam has left its aperture and passed a laser clean-up filter (300-340 nm, *AHF Analysentechnik*). The reference intensity is measured behind a beam splitter with a power

meter (Field Max II, *Coherent*), allowing for an on-line setting of the laser intensity. It then passes an electromechanic shutter, which executes the timing sequences "On" and "Off" for the UV illumination, and a $\lambda/4$-plate (quarter wave plate, QWP), generating circularly polarized light from the laser beam, which is linearly polarized. It is then focused through the back window of the cryostat by a quartz lens (f = 50 mm) to the sample.
A solid state laser diode with a wavelength of 488 nm (see Table A.2) is used for probing the fluorescence of the triads, as well as it induces the ring-opening reaction. After leaving its aperture, the beam is first sent through an assembly of OD glass filters and a continuous OD wheel, offering a wide range of intensity settings. It is then transferred to the microscope with a single-mode fibre, which acts as a useful tool for two functions. First, it makes the microscope input independent from the laser in front of the fibre, giving flexibility in the choice of the light source within the fibre specification. Second, it can easily be used for beam cosmetics, as its output is a Gaussian beam [124]. Behind the fibre, the beam passes the shutter for the timing of visible illumination before it reaches a Glan-Taylor prism (GTP) [124], selecting vertical polarization and thus transferring linearly polarized light. The other polarization also features one important purpose: it serves as the temporal reference for the timing sequence of the 488 nm light and is recorded by a photodiode (PD, S2387, *Hamamatsu*, wired by the Electronics Workshop of the University of Bayreuth). Then, the beam passes a 50/50 beam splitter cube, where its intensity reference is recorded, and a laser clean-up bandpass filter (BP, 483-493 nm, *AHF Analysentechnik*). Subsequently, a Berek polarization compensator, which is set as $\lambda/4$-plate (quarter wave plate, QWP), generates circularly polarized light in order to be able to excite all excitation dipole moments of the triads in the sample plane. Before passing the dichroic beam splitter (BS, DCXRU525, *AHF Analysentechnik*), a wide-field lens (WFL) can be flipped in or out of the beam for the choice of wide-field or confocal mode of the microscope, respectively. When flipped in, the excitation beam is not parallel anymore and causes an illuminated spot of $\approx$60 μm on the sample, enabling a choice of a single fluorescent spot for the measurements in confocal mode. This choice is done by a motorized, cardanic-mounted mirror in front of the microscope objective. The pivotal point of this mirror is then imaged to the back aperture by a telecenctric lens system (TL) (two lenses with f = 100 mm), thus avoiding optical aberrations like astigmatism or coma [124]. The objective itself is a long working distance objective (M Plan APO, 50x, NA = 0.55, infinity corrected, Edmund Optics, in Figure 4.3 denoted by the small lens in front of the cryostat) which focuses through the front window of the cryostat and a fused silica half sphere (diameter 5.0 mm, refractive index n = 1.52, Edmund Optics) serving as a SIL [67, 128] onto the sample. The fluorescence is collected by the same optic system and transferred back to the dichroic mirror and passes it this time, as well as

another bandpass filter (BP, HQ 525 BP, transmission 525-725 nm, *AHF Analysentechnik*) in order to remove residual stray light from the probe laser diode. A flippable mirror then gives the choice to detect the signal either with an EMCCD camera (Electron-Multiplying Charge-Coupled Device, iXon DV877ECS, *Andor*) or with an avalanche photodiode (APD, MPD5CTC, *PicoQuant)*). The former is used with the widefield lens flipped in, the mode of the microscope where a single emitter can be selected. The latter is used in confocal mode, in order to detect the signal from single triads.
The signal is recorded by a microprocessor system (ADWin, ADWin Gold II, *Jäger Messtechnik*), which stands out due to its real-time processing capabilities. At the same time, it serves for the timing of the sequential illlumination by controlling the shutters. From the microprocessor, the data is collected with a computer, which uses a LabView surface for the control of the microprocessor [111], and stored in ASCII-files for analysis.

4.3. Cryostat

Cryostat Equipment

The cryostat used for the measurements on single triads is a flow-type cryostat (KONTI-Cryostat Micro, *CryoVac*) see Figure 4.4.
Such a cryostat serves as a thermostat for temperatures between room temperature and low temperatures down to ≈ 5 K, which is achieved by the combination of a flow of helium for cooling, and a heater to regulate and stabilize the temperature. A vacuum pump (ME 4 NT, *Vacuubrand*, denoted by "He Pump" in Figure 4.4) draws helium from a vessel through the inner heat exchanger (IHE) of the cryostat, where the sample holder (SH, also called "cold finger") can be screwed in. After the cold helium has passed this heat exchanger, it pre-cools another outer heat exchanger (OHE) surrounding the central one and then leaves the cryostat, being stored for re-compression and liquefaction. In order to suppress thermal conduction and convection, a vacuum pump assembly consisting of a forepump and a turbomolecular pump (PT70F-Compact, *Leybold Vacuum*) evacuates the interior of the cryostat to 10^{-6} mbar. This pressure can be further lowered to $\approx 10^{-7}$ mbar by cooling down, making the cold interior of the cryostat act as a cryo pump. The evacuation features the positive side-effect that the sample is not exposed to oxygen, which would promote - in combination with UV illumination - photobleaching and deterioration of the sample and its matrix. Heat transfer into the cryostat through thermal radiation is at least decreased by the fact that the heat exchangers consist of brass with a polished surface, reflecting thermal radiation, as well as a heat shield which is installed as a cover shield for the cold parts of

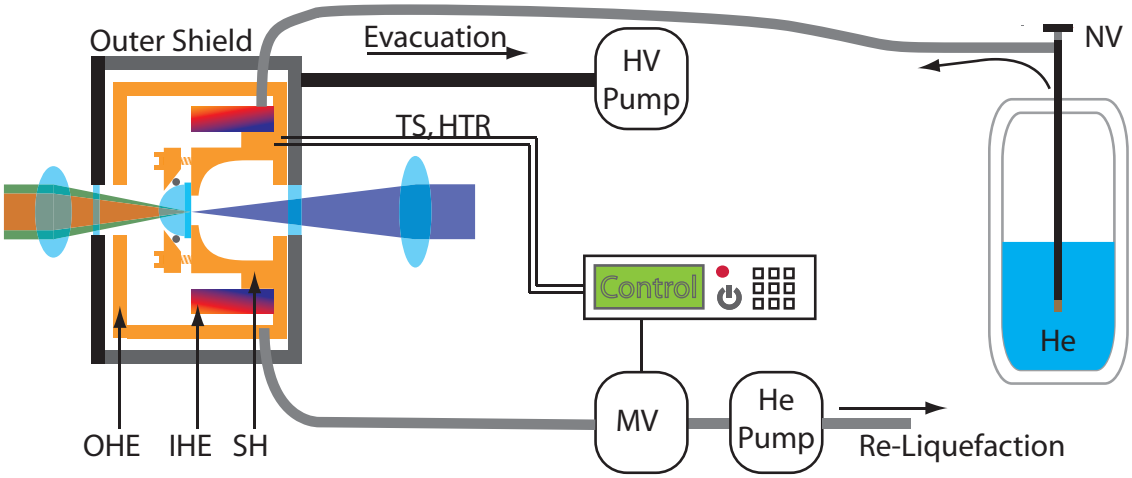

Figure 4.4.: *The Cryostat setup and its control components. Liquid helium (He) is drawn from a vessel by the helium pump (He Pump) and injected into the inner heat exchanger (IHE) of the cryostat, which had been evacuated by a turbomolecular pump (High Vacuum HV Pump). There, the sample holder is cooled to cryogenic temperatures, temperating the sample attached to it. After the helium has left the inner heat exchanger, the exhaust gas pre-cools the outer heat exchanger (OHE), which also serves as a heat shield and then leaves the cryostat. The control unit regulates the cryostat setup, as it monitors the temperature with a temperature sensor (TS) and and uses the signal for adjusting the magnetic valve (MV) to control the helium flow, and a heater (HTR) to fine-tune the temperature. The needle valve (NV) on the helium injector can be used to manually set the helium flow.*

the cryostat.

By using vacuum pumps, mechanical vibrations can easily be transferred to the optical setup, causing misalignment. These vibrations were damped effectively by laying the corrugated hose for the turbomolecular pump through a box containing sand bags. The helium pump makes use of a similar setup: it draws the helium through a massive cylinder which is damping vibrations.

Liquefied helium contains, to a certain extent, other gases like nitrogen or hydrogen. This fact becomes a problem when helium is drawn from a vessel, as the fine tubes inside the cryostat tend to block from these contaminations. This fact is circumvented by using a small sintered body which is screwed to the helium injector, serving as a filter and causing the blocking, if so, already there.

Operation

In this section, the detailed settings for the operation of the cryostat are presented, with the parameter denoted like in the controller unit of the cryostat. In order to achieve low temperatures, a flow cryostat uses a flow of cold gas on the one hand, and a small electric heater in the interior on the other hand. As a third controlling instrument, a magnetic valve can also limit the flow of helium.

This way, any temperature between 5 K and room temperature can be set easily and precisely. To control the flow of helium, a needle valve at the helium injector is set manually so that the manometer after the cryostat indicates a constant pressure of $200-250$ mbar. Then the electric heater can be programmed, making use of a proportional/integral/differential controller (PID-controller), where the time constants are set to 25 s and 5 s for the integral and the differential controller, respectively. For the 10 K operation, the heating BIAS voltage is set to 2 V, and the VARIABILITY is set to 30%, giving the heater a modulating range from 1.4 V to 2.6 V and resulting in a temperature deviation of ± 0.05 K when read from the cryostat controller. Higher temperatures up to ≈ 50 K are obtained by still leaving the helium constant as above, only enhancing the BIAS voltage to up to 10 V, and readjusting the VARIABILITY percentage. All these temperature settings are done with a fully opened magnetic valve (BIAS at 10 V, VARIABILITY at 0%). Going higher than 50 K, two more things come into play. First, the helium flow can be lowered slightly with the needle valve to 150 mbar with the side effect of saving helium. Second, the magnetic valve is also programmed to be run by the PID-controller. Here, the BIAS is set to 5 V with a VARIABILITY of 100% and the time constants of 10 s and 1 s for the integral and the differential controller, respectively.
The measurements were carried a fixed temperature of 10 K in the measurements for the chapters dealing with switching of single triads, Chapters 5 and 6.

4.4. Sample Preparation

For the sample preparation, circular coverslips were used, which are cleaned with acetone and methanol before residuals of these solvents were removed by burning. The same way, the small vials for the storage of solutions and chemicals were treated in order to remove contaminants which affect measurements in the fluorescence microscope.
The triads were obtained from the group of Prof. Dr. M. Thelakkat as powders, and stored in the dark in a refrigerator for the use. From these powders, initial solutions were prepared.

Single-Molecule Samples

First, a solution of poly(methyl methacrylate) (PMMA) in trichloromethane (common name: chloroform) was prepared with a concentration of 10 mg PMMA per 1 ml chloroform. From this solution, a sample was spincoated (2000 rpm, 60 s) and examined in the fluorescence microscope in widefield mode under settings later also used in the experiments (e. g. for the case of highest intensities $I_{488} = 200 W/cm^2$ and $I_{325} = 1.78 W/cm^2$).

Sample Preparation

This preliminary measurement served as a test to see if the solvent or the matrix was contaminated with fluorescent particles during preparation. In the case when fluorescent spots were clearly visible on the widefield image, the preparation of the matrix had to be redone, as these fluorescent spots cannot be distinguished from fluorescent triads later.
In the next step, solutions of triads were prepared. For the measurements presented in Chapter 5 and 6 *Triad 2* and *Triad 3* were used. The initial solutions contained triads and chloroform with a concentration of 4.4×10^{-5} mol/l, and were further diluted to a concentration of about 4.4×10^{-10} mol/l. This solution was mixed with the solution containing PMMA in equal parts (vol/vol), yielding solutions of triads with a concentration of 2.2×10^{-10} mol/l. From these solutions, 50 μl were spincoated on a microscope coverslip (2000 rpm, 60 s).

5. Single Molecule Experiments I - Single Triads and their Switching Behaviour

The experiments and interpretations in this chapter are published in
Johannes Maier, Martti Pärs, Tina Weller, Mukundan Thelakkat and Jürgen Köhler: "Deliberate Switching of Single Photochromic Triads", Sci. Reps. 7 (2017), 41739; see [106]
This chapter closely follows and in wide parts cites this publication.
The triads used for the experiments were kindly provided by the workgroup of Prof. Dr. Mukundan Thelakkat, University of Bayreuth.

5.1. Introduction

This chapter takes into account the considerations made in chapters 2 and 3. The DCP-PBI triads (**Triad 2**) are embedded in a poly(methyl methacrylate) (PMMA) matrix and cooled down to 10 K, serving for a slowed cycloreversion reaction and by the way providing an oxygen-free environment in the cryostat. This inhibits undesired irreversible photobleaching.

5.2. Results

In order to locate the individual triads the sample was excited at 488 nm and a fluorescence image was recorded using a low-temperature widefield microscope. Subsequently, a single triad was selected from the image and the microscope was switched to confocal mode. From our experiments we find that only a fraction of about 30% of the investigated triads showed reversible switching between a high- and a low-fluorescent state upon illumination with UV and visible radiation. This is ascribed to the fact that the DCP units can take two conformations, parallel and antiparallel, and that only the antiparallel conformation can undergo the photocyclization [103]. In the following we will focus on those triads that

allowed for a light-induced modulation of the fluorescence intensity.

5.2.1. The Switching Experiment

In the first experiment we verify the light-induced switching of a single triad between a low- and a high-fluorescent state, and test the fatigue resistance. Therefore, a single triad is illuminated for 1 s at 325 nm with a fixed intensity of $1.78 W/cm^2$. This initialises the triad in a state with a closed DCP unit, corresponding to the state with reduced fluorescence intensity from the PBI units [21, 61]. Then, after a waiting time of 1.3 s without any illumination the probe laser at 488 nm is switched on for 0.5 s. Radiation at this wavelength serves for both, conversion of the DCP to the open state and probing the fluorescence of the PBI units. After another waiting time of 0.2 s without illumination the whole illumination sequence is repeated 8800 times corresponding to a total duration of the experiment of 26400 s (7h 20 min). It is worth noting that the end of the experiment after more than 7 hours was determined by the experimentalist and not due to a deterioration of the triad. During the experiment the fluorescence from the triad is sampled with a dwell time of 5 ms. The result of this experiment is exemplified in Figure 5.1 a) for three cut-outs of 20 s duration each from the full data set. The illumination sequences are indicated at the top of Figure 5.1 a) by the coloured bars. Expanded views of the rising edges of the fluorescence intensity after switching on the probe laser are shown in Figure 5.1 b-d) and reveal a delay of some ten milliseconds between the onset of the laser and the raise of the fluorescence.

5.2.2. The Distributions for the Fluorescence Delay Times and Rates

For the 8800 repetitively carried out switching sequences the distribution of these times is shown in Figure 5.2 a) and follows an exponential decay (orange line, Figure 5.2 a)). Given a temporal resolution of two times the dwell time, i.e. 10 ms, we note that the fraction of delay times longer than 10 ms amounts to about 95%.

In order to quantify our observations we represent the histogram of the delay times as a cumulative distribution function (CDF) defined as

$$CDF(\tau) = \frac{\sum_{t=0}^{t=\tau} N(t)}{\sum_{t=0}^{t=\infty} N(t)} \tag{5.1}$$

where N(t) denotes the number of events with a delay time t. The CDF(τ) corresponds directly to the probability to observe a change of the fluorescence intensity during the time interval $0 < t \leq \tau$. The respective CDF for the histogram shown in Figure 5.2 a) is

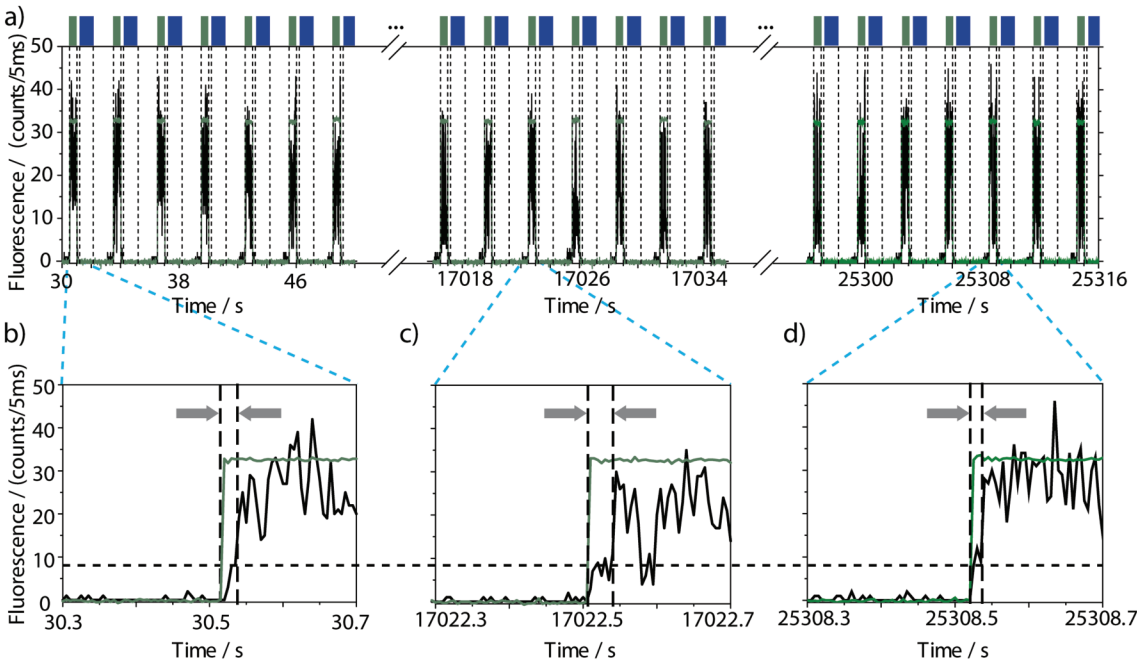

Figure 5.1.: *a) Cut-outs of the fluorescence response (black line) of a single triad as a function of the illumination with radiation at* 325 nm *(blue,* $I_{325} = 1.78 W/cm^2$*) and* 488 nm *(green,* $I_{488} = 120 W/cm^2$*) as indicated on top of the panel. The emission is sampled with a dwell time of* 5 ms*. Rising edges of individual switching cycles are shown in b), c) and d) on an expanded scale, where the temporal profile of the* 488 nm *illumination is given by the green line. The horizontal dashed line indicates the background level. Figure adapted from [106]*

displayed in Figure 5.2 b). It can be fitted by an asymptotic exponential growth of the type

$$CDF(\tau) = C_0 - C_1 \cdot e^{\frac{\tau}{\tau_{ON}}} \tag{5.2}$$

(orange line, Figure 5.2 b)), where C_0 and C_1 represent an offset and an amplitude, respectively, and τ_{On} represents the average delay time that will be referred to as switch-on-time hereafter. For the example shown we find τ_{On} = 75.7 ms. According to the model developed in [25], the switch-on-time can be associated with the close-to-open conversion rate k_{co} via $k_{co} = (\tau_{On})^{-1}$. The distribution of this rate is shown in Figure 5.2 c) for 35 experiments, carried out on 13 individual triads. For these experiments each single triad was exposed to 400 consecutive illumination sequences at similar excitation conditions as detailed above. The rates found for k_{co} range from $1.2 s^{-1}$ to $48.8 s^{-1}$ with a mean value of $10.7 s^{-1}$. This variation might be caused by differences in the quantum yield of the ring opening reaction among the individual triads due to different local environments, but more probably it reflects the different out-of-plane orientations of the transition-dipole moments of the individual triads with respect to the polarization of the incident light field, resulting in variations of the effective excitation intensity.

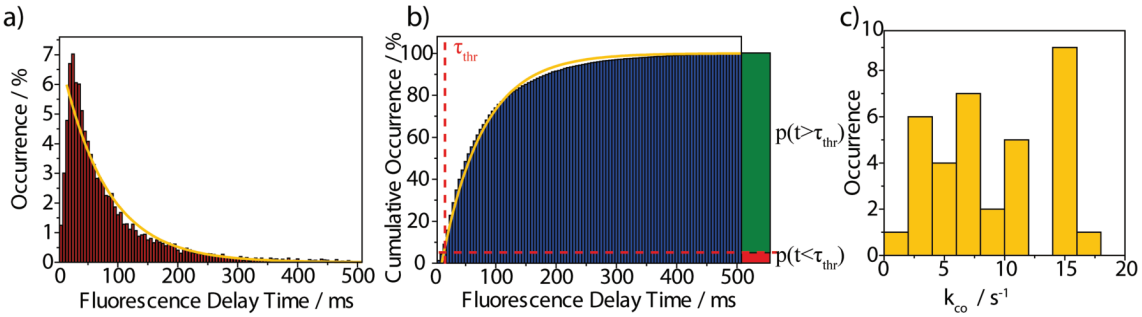

Figure 5.2.: *a) Relative and b) cumulative distribution of the delay times for 8800 illumination sequences. The orange lines correspond to an exponential decay (a), or asymptotic exponential growth (b), respectively. The vertical dashed line in (b) indicates the temporal threshold τ_{thr} that corresponds to twice the dwell time thereby setting the experimental time resolution. The horizontal dashed lines separate the probabilities $p(t < \tau_{thr})$ and $p(t > \tau_{thr})$ at the threshold, visualised by the red and green bars on the right hand side. c) Histogram of the ring-opening rate $k_{co} = (\tau_{On})^{-1}$ for 13 individual triads based on 35 experiments with 400 illumination sequences per triad. Figure adapted from [106]*

5.2.3. The Control Experiment and its Distributions of Delay Times

In order to verify that we deal indeed with photochromic switching of an individual triad rather than blinking, we performed for each triad under study a control experiment without exposing the molecule to the 325 nm beam and applied only the radiation at 488 nm. The corresponding data for the triad that has been used for Figures 5.1 and 5.2 are shown in Figure 5.3.

Now the onset of the fluorescence follows directly the modulation of the intensity of the excitation laser without delay, see 5.3 b). This is also evident from the histogram of the delay times, Figure 5.4 a) whose entries accumulate around time bins corresponding to time delays of 5 to 10 ms. Since our data acquisition runs with 5 ms sampling time, this reflects simply the achievable temporal resolution of the experiment, i.e. two time bins.

The corresponding CDF is displayed in 5.4 b) and is not compatible with the type of exponential function used before. However, closer inspection of the fluorescence time traces reveals also the typical blinking of single molecules, see for example the red dashed box in 5.3 b) after about 6.55 s. If such blinking events occur within the first 10 ms after switching on the probe beam these will be registered as a finite ”delay time”, which explains the entries in the range between 10 ms and 300 ms in the histogram 5.4 b). For the two-beam experiments such blinking events contribute as ”false positives” (vide infra) to the histogram of the delay times in 5.2 a) and b).

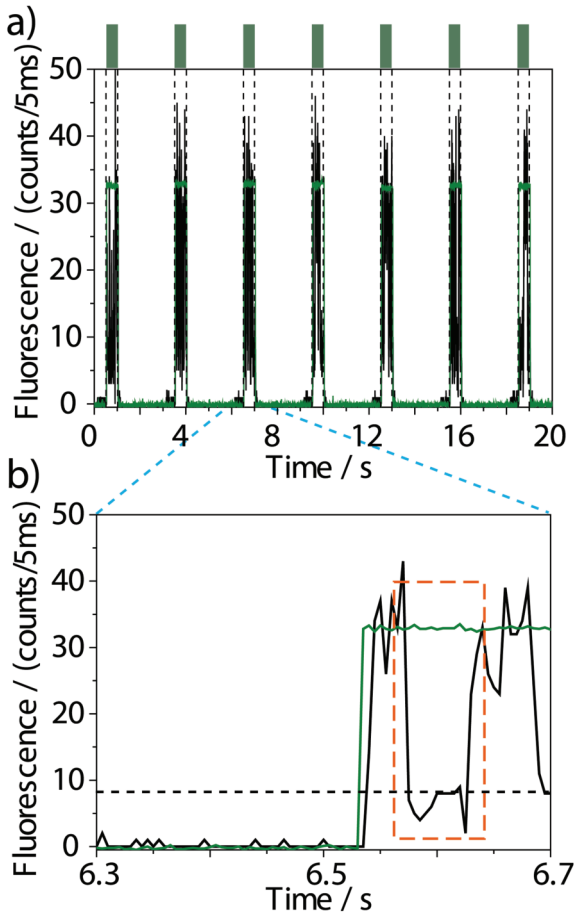

Figure 5.3.: *Control experiment on the same triad as used for 5.1 without 325 nm illumination. a) Cut-out of the fluorescence response (black line) as a function of the illumination at 488 nm (green) as indicated on top of the panel. The emission was sampled with a dwell time of 5 ms. b) Single illumination cycle on an expanded scale. The green line corresponds to the temporal profile of the 488 nm illumination. The horizontal dashed line indicates the background level. The red dashed box empasizes a blinking event.Figure adapted from [106]*

5.2.4. The Dependence on the probe beam intensity

Next we studied the switching behaviour of an individual triad as a function of the intensity of the probe beam at 488 nm. Therefore this intensity was varied between $59W/cm^2$ and $200W/cm^2$, and in each experiment the single triad was exposed to 400 illumination sequences. The resulting CDFs are shown in 5.5 and can all be described by an asymptotic exponential growth of the form $CDF(\tau) = c_0 - C_1 \cdot e^{\frac{-\tau}{\tau_{On}}}$. For the corresponding switch-on-times we find τ_{On} = 57.1 ms ($59W/cm^2$), 66.4 ms ($78W/cm^2$), 27.3 ms ($100W/cm^2$), and 15.2 ms ($200W/cm^2$), respectively, featuring a monotonic decrease for increasing the 488 nm intensity above $78W/cm^2$.

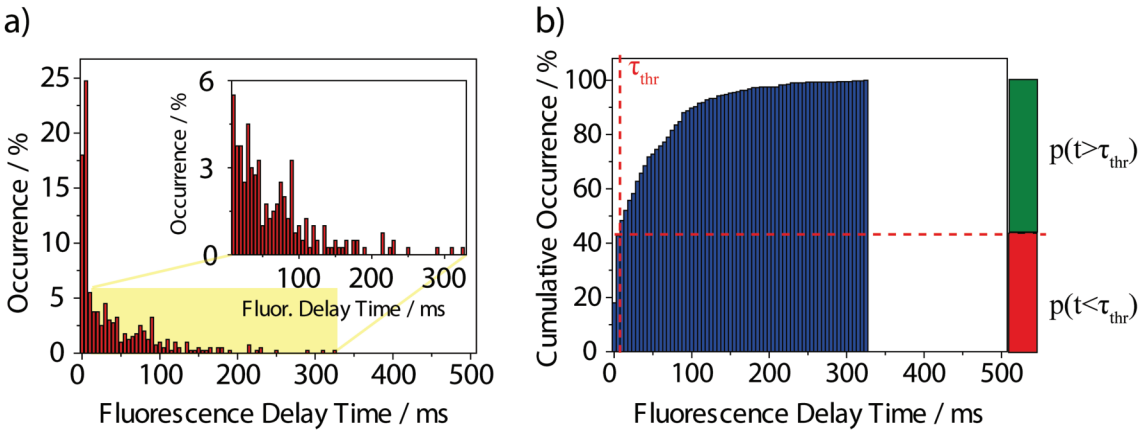

Figure 5.4.: *Histograms of fluorescence delay times for the same triad as used for 5.1, without* 325 nm *illumination. a) Relative distribution of the delay times for 400 illumination sequences. The inset shows the yellow shaded area on an expanded scale. b) Cumulative distribution function of the delay times for an excitation intensity of* $120W/cm^2$ *at 488 nm. The vertical dashed line indicates the temporal threshold* τ_{thr} *that corresponds to the experimental time resolution. The horizontal dashed line separates the probabilities* $p(t < \tau_{thr})$ *and* $p(t > \tau_{thr})$ *at the threshold, red and green bars, respectively. All experiments were carried out at 10 K. Figure adapted from [106]*

5.2.5. Fluorescence Counts and their Distribution

For the reference experiments that address the blinking of individual triads, these were illuminated solely with the radiation at 488 nm. For analysing the blinking statistics of the triad used for Figures 5.1, 5.3 and 5.5 a-c), the data from the control experiment were appended, which yields a fluorescence intensity trace of 200 s duration. An excerpt of this trace is shown in Figure 5.6 a) revealing the typical telegraph-like blinking of single molecules.

The distribution of the intensity levels of the full trace is shown in 5.6 b) and features two peaks. The lower one has a maximum at 8 counts /5 ms (1600 counts / s) and corresponds to the background level (see also Figure 5.1 b-d), 5.3 b) in the main text), whereas the higher one peaks at 27 counts /5 ms (5400 counts / s) and corresponds to the average intensity of the ON state. We used the minimum between these two peaks for discriminating the ON and the OFF levels (see dashed line in Figure 5.6). This yields about equal fractions for the residence times in those states, i.e. $T_{OFF}/T = 50.4\%$ and $T_{ON}/T = 49.6\%$. Here T_{ON} (T_{OFF}) refers to the total accumulated residence time in the ON (OFF) level, and T to the total time of the experiment.

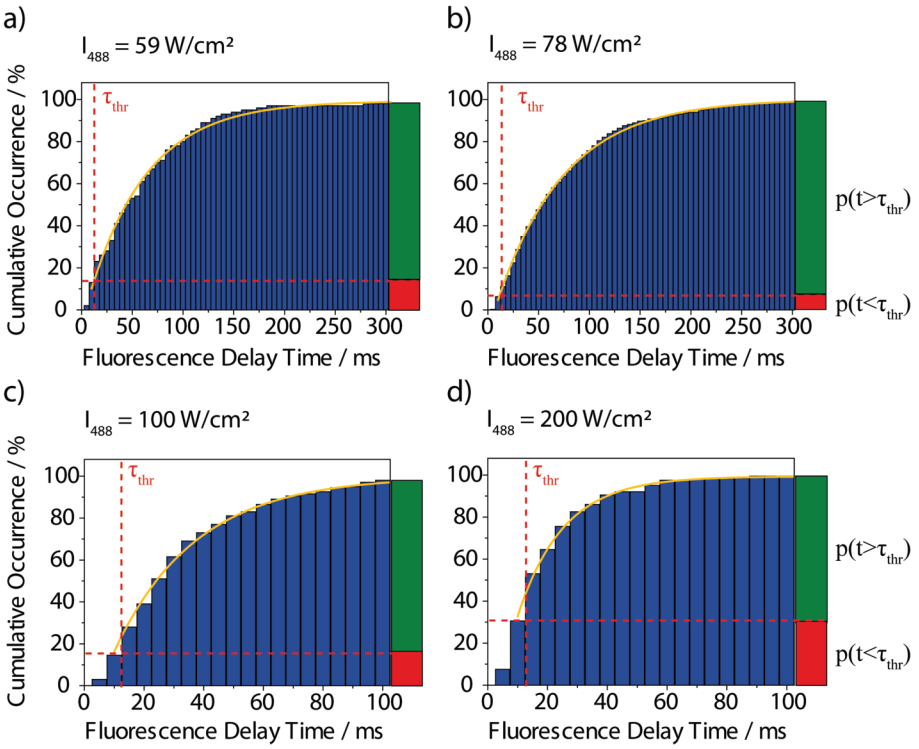

Figure 5.5.: *Cumulative distribution functions of the fluorescence delay times as a function of the* 488 nm *excitation intensity: a)* $59W/cm^2$*; b)* $78W/cm^2$*; c)* $100W/cm^2$*; d)* $200W/cm^2$*. All distributions correspond to experiments with 400 consecutive illumination sequences. The data have been sampled with dwell times of 10 ms (a,b) and 5 ms (c,d), respectively. Note the different scales in a,b versus c,d. The orange lines correspond to an asymptotic exponential growth, whereas the vertical dashed lines indicate the temporal threshold* τ_{thr} *that corresponds to twice the dwell time thereby setting the experimental time resolution. The horizontal dashed lines separate the probabilities* $p(t < \tau_{thr})$ *and* $p(t > \tau_{thr})$ *at the threshold, visualised by the red and green bars on the right hand side. The experiments were carried out at* 10 K *on the same single triad. Figure adapted from [106]*

5.3. Discussion

For the two-beam experiment the DCP is initialised in the closed state (low PBI fluorescence yield) and illumination at 488 nm first converts the DCP to the open state before the PBI fluorescence with high emission yield is initiated. Generally, both the light-induced conversion of the photochromic unit and the emission of a photon from the PBI are quantum mechanical processes that obey Poissonian statistics, like illustrated in Section 3.6.2. However, the typical time scale for the processes is in the pico- and nanosecond range, respectively, which is beyond the temporal resolution of our experiment, and we can only observe the time the triad cycles the excitation in its closed state. As a consequence of the Poissonian statistics for the light-induced conformational change, the distribution for finding a delay time in the interval between τ and $\tau + d\tau$ is given by an exponential decay. As can be seen from Figure 5.2 a) the data are clearly in line with this expectation.

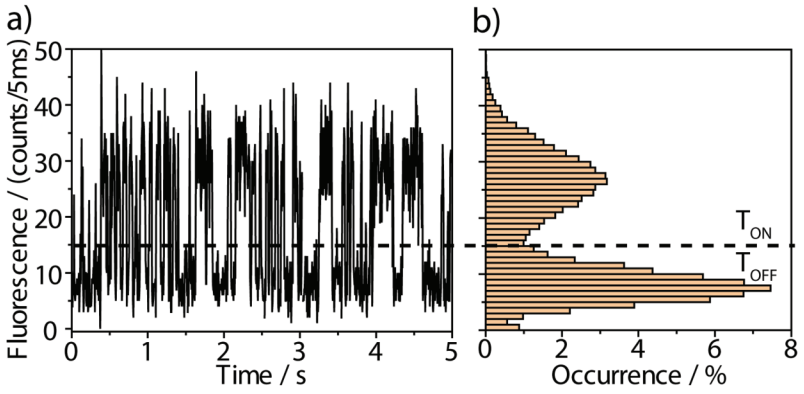

Figure 5.6.: *a) Excerpt of a fluorescence intensity trace from a single triad. The trace has been constructed from the fluorescence patches obtained in the control experiment described in Figure 5.3 a) of the main text. Given the 400 illumination cycles of 0.5 s duration each, this amounts to a total length of the trace of 200 s. b) Distribution of the intensity levels for the full fluorescence intensity trace. The dashed line indicates the threshold used to discriminate between the "On" and the "Off" state. Figure adapted from the Supporting information of[106]*

Mathematically the distribution for the delay times corresponds to a probability density, and its integral, here presented as the CDF(τ), gives directly the probability for observing a switching event during the time interval $[0,\tau]$.
Hence, for the current situation the CDF is expected to have the form

$$CDF\,(\tau) = C_0 - C_1 \cdot e^{\frac{\tau}{\tau_{ON}}} \tag{5.3}$$

which is also corroborated by the data, see Figure 5.2 b) and Figure 5.5. In contrast, for illumination at 488 nm only, the DCP unit is already preinitialised in the open state. This explains why, given the temporal resolution of the experiment, the onset of the fluorescence promptly follows the rising edge of the laser intensity.
Accordingly, the experimentally accessible readout values for the onset of the fluorescence are either "delay zero" or "finite delay". However, due to the unavoidable blinking, see Figure 5.3, a delayed onset cannot directly be associated with a deliberate switching of the photochromic unit, and we have to resort to the concept of conditional probabilities to quantify our results. Let S (S for switching) refer to the event that the triad is initially prepared in the closed state and that it undergoes a conformational change to the open state upon irradiation with 488 nm, and let $\bar{S}$ refer to the event that the triad does not change its intial conformational state. Analogously, let "+" refer to the event "registration of a finite delay", and "-" denote the event "registration of delay zero", i.e. a prompt onset of the fluorescence. Then, for example, $p\,(+|S)$ refers to the conditional probability that we register a finite delay time given that the DCP underwent a conformational change from the closed to the open state ("true positive"). Likewise, $p\left(+\middle|\bar{S}\right)$ denotes the conditional

probability that we register a finite delay time (for example due to blinking) under the condition that the DCP did not change its conformation (”false positive”). Defining a temporal threshold, τ_{thr}, that takes our temporal resolution into account, allows us to read probabilities for registering specific events from a single molecule directly from the CDFs in Figure 5.2b), Figure 5.5. For example, the green bar on the right hand side of Figure 5.2 b) indicates the probability for registering finite delay times $p(t > \tau_{thr})$ irrespective whether the DCP underwent a conformational change or not. This represents to the total probability to register a finite delay time given as [133]

$$p(t > \tau_{thr}) = p_E(+) = p_E(+|S) \cdot p_E(S) + p_E\left(+\middle|\bar{S}\right) \cdot p_E\left(\bar{S}\right), \tag{5.4}$$

where $p_E(S)$ refers to the probability for a conformational change of the DCP from the closed to the open state, and $p_E\left(\bar{S}\right) = 1 - p_E(S)$ refers to the probability that the DCP does not change its conformation. The index E refers to the experimental situation with two laser beams. For the CDF from the control experiment displayed in Figure 5.3 d) the situation is slightly different. From the design of the control experiment we know by definition that the DCP unit will not undergo a light-induced change of its conformation, $p_C(S) = 0$. Hence, here $p(t > \tau_{thr})$ corresponds to the conditional probability that we register a finite delay time under the condition that the molecule did not change its conformational state, i.e

$$p(t > \tau_{thr}) = p_C\left(+\middle|\bar{S}\right). \tag{5.5}$$

Here the index C refers to the control experiment. However, the interesting statistical parameter is the PPV, $p_E(S|+)$, i.e. the probability that the triad indeed underwent a conformational change given that we have registered a finite delay. Using the expression for the total probability $p_E(+)$ and applying Bayes law [133] this yields

$$PPV = p_E(S|+) = \frac{p_E(+) - p_E\left(+\middle|\bar{S}\right) \cdot p_E\left(\bar{S}\right)}{p_E(+)} = 1 - \frac{p_E\left(+\middle|\bar{S}\right) \cdot p_E\left(\bar{S}\right)}{p_E(+)} \tag{5.6}$$

The conditional probability $p_E\left(+\middle|\bar{S}\right)$ can be read from the CDF in Figure 5.4 b) using the approximation $p_E\left(+\middle|\bar{S}\right) \cong p_C\left(+\middle|\bar{S}\right)$, and a quantitative estimate for $p_E\left(\bar{S}\right)$ can be obtained as T_{OFF}/T from the data which concern solely the blinking behaviour of the triad under study, see Figure 5.6. Using the figures obtained from the experiments ($p_C\left(+\middle|\bar{S}\right) = 0.57$, $p_E(+) = 0.96$, and $p_E\left(\bar{S}\right) = 0.50$) this yields a positive predictive value of 0.70.

In Figure 5.7 a) the distribution of the PPV is shown for 15 single triads that were studied for 400 illumination sequences each, using $I_{325} = 1.78W/cm^2$ and $I_{488} = 200W/cm^2$. As blinking reference data, each triad was illuminated continuously at 488 nm for 100 s with

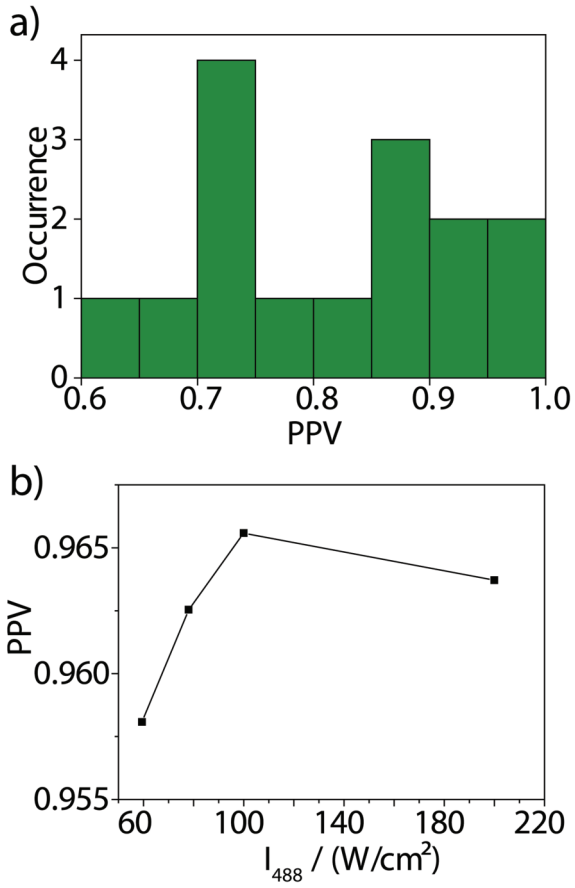

Figure 5.7.: *a) Distribution of the positive predictive values $p_E(S|+)$ for 15 individual PBI-DCP-PBI triads, initialised with $I_{325} = 1.78W/cm^2$, and probed with $I_{488} = 200W/cm^2$. b) Positive predictive value $p_E(S|+)$ for one selected individual PBI-DCP-PBI triad as a function of the intensity of the probe beam. Figure adapted from [106]*

the same intensity as for the corresponding photoconversion experiment. The analysis for $T_{OFF}/T = p_E\left(\bar{S}\right)$ then followed the same strategy as shown in Figure 5.6.

The obtained ppvs range from 0.62 to 0.97 centred at 0.81 ± 0.11 (mean $\pm$ stdev). For one of the triads that featured a relatively large PPV of 0.964, we studied as well the ppv as a function of the intensity of the probe beam, Figure 5.7 b). This reveals only a weak variation of this parameter between 0.958 and 0.965 for changing the intensity I_{488} between $60W/cm^2$ and $200W/cm^2$, featuring a peak value of 0.965 for $I_{488} = 100W/cm^2$.

We have shown that the particular photochromic triad system features excellent fatigue resistance with high contrast between the detected signals in the two light induced conformations. Exploiting the high fluorescent yield of the perylene based chromophores attached to the photochromic unit allows to observe photochromic switching at the single molecule level. We verified that the probability to observe deliberate light-induced switching processes rather than stochastic blinking processes from a single triad is on average about 80%, and can exceed 95% in a few exceptional cases. These numbers are sufficiently

large for application in sensitive biosensing, and super-resolution imaging [134]. However, for optical data storage these numbers are far too small, and further research is required to elucidate the key parameters that finally determine the actual value of the positive predictive value.

6. Single Molecule Experiments II: Long-term behaviour and different fluorophores

This chapter forms the basis for the manuscript of the publication
Johannes Maier, Tina Weller, Mukundan Thelakkat and Jürgen Köhler: "Long-term switching of single photochromic triads based on dithienylcyclopentene and fluorophores at cryogenic temperatures", J.Chem.Phys. 155, (2021), 014901; see [135].
This chapter closely follows and in wide parts cites this publication.
The triads used for the experiments were kindly provided by the workgroup of Prof. Dr. Mukundan Thelakkat, University of Bayreuth.

6.1. Introduction

In this chapter, the single molecule measurements are continued. Next to the aforementioned DCP-PBI triad (**Triad 2**), additionally a DCP-BODIPY triad (**Triad 3**) is examined, again in low temperature, oxygen-free conditions. And also the measurement strategy is slighly different to the one applied in Chapter 5. Now, for each switching experiment, one control experiment was performed. This enables the observation of the PPV in dependence of the number of repetitions of the switching/control experiment pair.

6.2. Results and Discussion

6.2.1. Switching Experiments for Single Triads DYE-DCP-DYE and their Cumulative Histograms

For the single molecule experiments the selected triad is exposed to radiation at 325 nm with an intensity of $1.78 W/cm^2$ for 1 s, which initialises the triad in the low-fluorescent state. This period is followed by a waiting time of 0.3 s without exposure to light, and subsequent illumination at 488 nm for 0.5 s with an intensity of $200 W/cm^2$. Prior to the

next illumination with UV light there is another waiting time of 0.2 s. In the following the whole sequence - 1 s (325 nm) - 0.3 s (no light) - 0.5 s (488 nm) - 0.2 s (no light) - will be referred to as one switching cycle. Thereby, the radiation at 488 nm serves for both, inducing the photocycloreversion reaction and probing the fluorescence of the dyes. In the following, the arrangement of figures will always follow a fixed pattern, with data for the **Triad 2** (PBI-DCP-PBI) shown on the left, and **Triad 3** (BODIPY-PBI-BODIPY) shown on the right.

For each type of triad an example of a single switching cycle is cut-out from a full data set

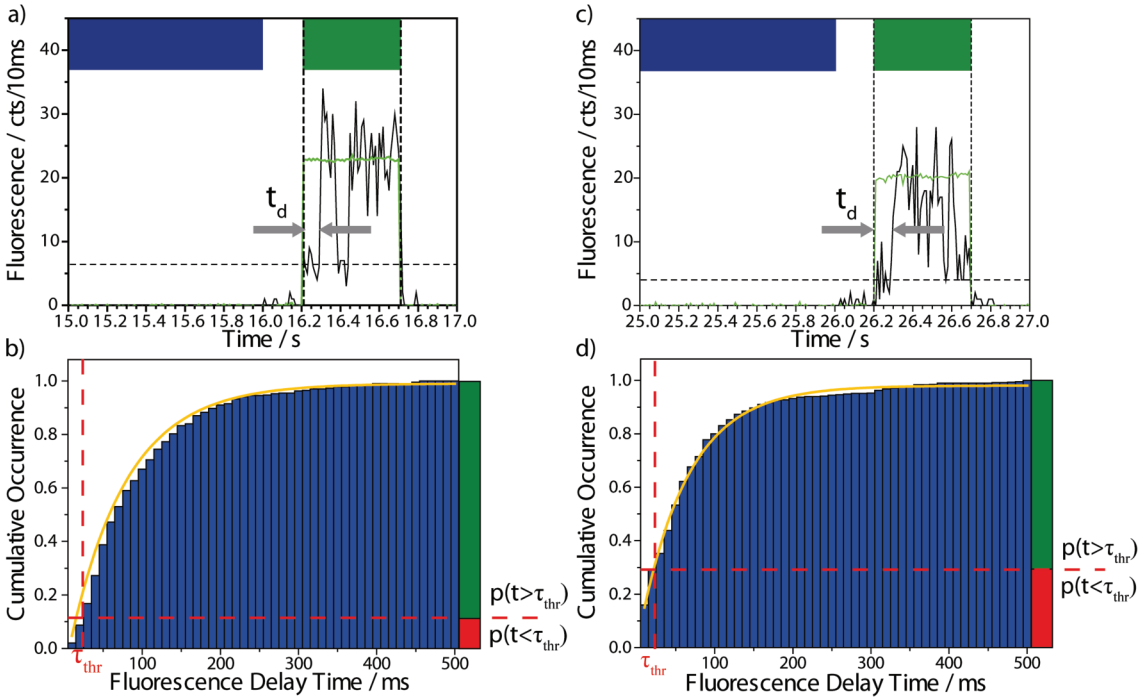

Figure 6.1.: *left a), b) PBI-DCP-PBI, right c), d) BODIPY-DCP-BODIPY.*
*a),c) Cut-outs of the response of single triads to a single illumination cycle [*1 s *(*325 nm*, 1.78* W/cm^2*)* - 0.3 s *(no light)* - 0.5 s *(*488 nm*, 200* W/cm^2*)* - 0.2 s *(no light)] as indicated by the coloured bars at the top. The emission of the triads is sampled with a dwell time of* 10 ms*. The rising edge of the* 488 nm *illumination is shown by the first dashed vertical line. The green line corresponds to the laser intensity and the black line corresponds to the signal. The delay,* t_d*, of the onset of the fluorescence with respect to the onset of the excitation laser is indicated by the thick grey arrows. The horizontal dashed line corresponds to the background level. b),d) Cumulative distributions of the delay times* t_d *for 400 switching cycles. The yellow lines correspond to fits to an asymptotic exponential growth (see text) with time constants of* 72.9 ms *(left) and* 61.7 ms *(right), respectively. The vertical red lines indicate the temporal thresholds,* τ_{thr}*, which is twice the dwell time. The horizontal red lines separate the probabilities* $p(t < \tau_{thr})$ *and* $p(t > \tau_{thr})$ *at the threshold depicted by the red and green bars at the right hand side. Here we have b)* $p(t < \tau_{thr}) = 0.0875$ *and* $p(t > \tau_{thr}) = 0.9125$*, g)* $p(t < \tau_{thr}) = 0.2925$ *and* $p(t > \tau_{thr}) = 0.7075$*.*
All experiments were carried out at a temperature of 10 K. Adapted from [135]

of switching cycles and shown in Figure 6.1 a)(PBI-DCP-PBI triad) and c) (BODIPY-DCP-BODIPY triad). The illumination sequence is depicted by the coloured bars on top of the

panels (blue: 325 nm; green: 488 nm), and the resulting fluorescence from the dyes as a function of time is shown by the black lines. This reveals that the onset of the fluorescence is delayed with respect to the onset of the 488 nm illumination as indicated by the thick grey arrows in Figure 6.1 a) and c) and referred to as delay time t_d. This can be quantified by defining $N(t_d)$ as the number of observed events with delay time t_d, and resorting to the cumulative distribution function (CDF) defined as

$$CDF(\tau) = \frac{\sum_{t_d=0}^{t_d=\tau} N(t_d)}{\sum_{t_d=0}^{t_d=\infty} N(t_d)}. \tag{6.1}$$

The $CDF(\tau)$ is directly related to the probability to find a delay time for the fluorescence intensity within the time interval $0 < t_d \leq \tau$. The $CDFs$ corresponding to the full experiment of 400 switching cycles for each triad are shown in Figure 6.1 b) and d) and can be fitted according to $CDF(\tau) = 1 - e^{-\frac{\tau}{\tau_{On}}}$ (orange lines).
Here τ_{On} represents the average delay time for the onset of the fluorescence for the particular triad. For the examples shown, the fits yield τ_{On} = 72.9 ms for PBI-DCP-PBI (Figure 6.1 b)), and τ_{On} = 61.7 ms for BODIPY-DCP-BODIPY (Figure 6.1 d)), respectively.

6.2.2. Control Experiments for Single Triads DYE-DCP-DYE and their Cumulative Histograms

In order to discriminate between unavoidable blinking and deliberate switching we performed for each triad a control experiment which was identical to the initial experiment, yet without the UV illumination.

The results are shown in 6.2 a) and d), and it becomes evident that now the onset of the fluorescence follows directly the onset of the intensity of the 488 nm radiation without further delay. The corresponding $CDFs$ are shown in Figure 6.2 b) and e) and are not consistent with the fit function used above. A closer look (see the red dashed boxes) at the fluorescence time traces in Figure 6.2 a) and d), uncovers blinking events at 24.45 s (Figure 6.2a)) and 36.55 s (Figure 6.2 d)), respectively, that are typical for single molecules. If similar blinking events would occur during the first dwell time in a two-beam experiment these will contribute as "false positives" to the $CDFs$ of the delay times as shown in Figure 6.1 b) and d). Finally, Figure 6.2 c) and f) addresses solely the blinking behaviour of the triads. The fluorescence intensity as a function of time has been obtained by appending the data from the control experiments resulting in a fluorescence time trace of 200 s duration. Cut-outs of these traces are shown in Figure 6.2 c), f) and feature the typical telegraph-like blinking of single molecules. The distributions of the intensity levels of the full trajectories

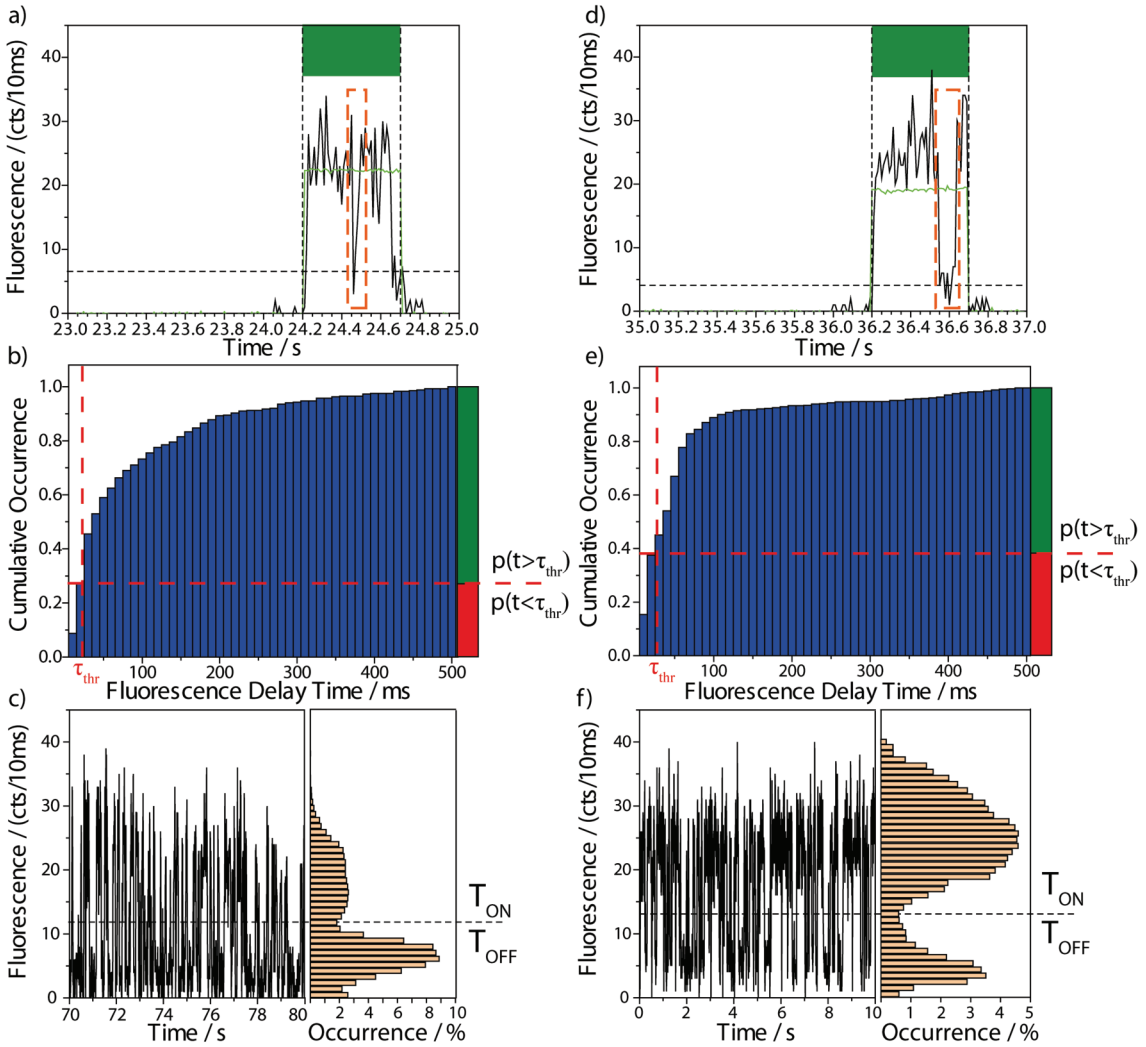

Figure 6.2.: *left a), b), c) PBI-DCP-PBI, right d), e), f) BODIPY-DCP-BODIPY. a),d) Control experiments: Cut-outs of the response of single triads to a single illumination cycle without UV illumination [*1 s *(*325 nm*, -)* - 0.3 s *(no light)* - 0.5 s *(*488 nm*, 200* W/cm^2*)* - 0.2 s *(no light)] as indicated by the green bar at the top. The further setup of the panels is similar to that Figure 6.1 a) and c). The dashed red boxes emphasize reversible drops of the fluorescence intensity at about* 24.45 s *(left) and about* 36.55 s *(right). b),e) Cumulative distributions of the delay times* t_d *for 400 switching cycles of the control experiments shown in a),d). The further setup of the panels is similar to that of Figure 6.1 b),d).Here we have b)* $p(t < \tau_{thr}) = 0.2725$ *and* $p(t > \tau_{thr}) = 0.7275$*, e)* $p(t < \tau_{thr}) = 0.375$ *and* $p(t > \tau_{thr}) = 0.625$*. c), f) Cut-out from fluorescence intensity traces (total length:* 200 s*) from single triads. The traces have been constructed by appending the fluorescence patches obtained in the control experiments shown in a),d). The distributions of the intensity levels of the total intensity traces are displayed at the right hand side of the blinking traces. The dashed horizontal lines correspond to the threshold for discrimination between ON and OFF. All experiments were carried out at a temperature of 10 K. Adapted from [135]*

are shown next to the intensity traces from which we find $T_{OFF}/T = 0.67$ (Figure 6.2 c)) and $T_{OFF}/T = 0.23$ (Figure 6.2 f)), where T_{OFF} refers to the accumulated residence time

in the off level and T to the total duration of the experiment.

6.2.3. Comparison of the Positive Predictive Values for the two Triads

For the two-beam experiment the photochromic DCP unit is initialised in the closed state, corresponding to the low-fluorescent state of the dyes. Both the light-induced conversion of the DPC unit and the emission of a photon from the dye molecule are probabilistic processes that follow Poissonian statistics. Given the temporal resolution of our experiment the emission process on the nanosecond time scale cannot be resolved. Hence we ascribe the delay times, t_d, observed for the onset of the fluorescence to the photocycloreversion reaction of the DCP units. Mathematically, the distribution of the delay times corresponds to the probability density to find a delay time t_d in the interval $\tau, \tau + d\tau$, and the probability to find a delay time in the interval [0, τ] is given by the $CDF(\tau)$. Owing to the underlying Poissonian statistics the $CDF(\tau)$ is expected to have the form $CDF(\tau) = 1 - e^{-\frac{\tau}{\tau_{ON}}}$ which is consistent with the data presented in 6.1 b) and d). For the control experiment, where only radiation at 488 nm has been used, the DCP is already preinitialised in the open state and, within the temporal resolution of the experiment, the onset of the fluorescence follows directly the rising edge of the laser intensity.
Obviously the experimental readout is either prompt or delayed onset of the fluorescence. Unfortunately, a delayed onset of the fluorescence cannot directly be associated with a light-induced switching of the DCP due to possible blinking, and we can only try to answer the question: What is the conditional probability $p(S|+)$ that the triad underwent a conformational change given that a delayed onset of the fluorescence has been observed. This conditional probability is also referred to as positive predictive value (PPV). Here "+" denotes the observation of a delayed onset of the fluorescence, and S refers to a light-induced switching event of a triad that was initially prepared in the closed state. Likewise $\bar{S}$ refers to an event that the triad has not changed its initial conformation, and $p\left(+|\bar{S}\right)$ to the conditional probability that a delayed onset of the fluorescence is observed although the conformation of the triad has not changed (false positive). Then $p(S|+)$ follows from the total probability for observing a delayed response $p(+) = p(+|S)p(S) + p(+|\bar{S})p(\bar{S})$ and the application of Bayes law [133] as

$$p(S|+) = 1 - \frac{p\left(+|\bar{S}\right) p\left(\bar{S}\right)}{p(+)} \tag{6.2}$$

The ingredients of this equation can be obtained from the $CDFs$ and the blinking experiment. The temporal resolution of our experiment is determined by twice the bin time that was used for registering the fluorescence from a single triad (here 2 x 10 ms), which prevents the registration of delay times t_d shorter than this interval. Yet, for longer times

the total probability $p(+)$ for registering a finite delay irrespective whether the DCP underwent a conformational change can be read directly from the *CDFs* in Figure 6.1 b) and d), as indicated by the green vertical bars. From the setup of the control experiment it is known beforehand that the DCP will not undergo a light-induced conformational change. Hence the conditional probability $p\left(+|\bar{S}\right)$ can be read from the *CDFs* in Figure 6.2b) and e), again indicated by the green vertical bars. Finally, a quantitative estimate for the probability $p(\bar{S})$ is provided by the blinking experiment (Figure 6.2 c) and f)). For the triads shown in Figures 6.1 and 6.2 we find for the PBI-DCP-PBI (BODIPY-DCP-BODIPY) triad $p(+) = 0.91$ (0.71), $p\left(+|\bar{S}\right) = 0.73$ (0.63), and $p(\bar{S}) =$ 0.67 (0.23), which yields for the PPV $p(S|+)$ $= 0.46$ (0.80). In other words, for the particular PBI-DCP-PBI (BODIPY-DCP-BODIPY) triad used for Figure 6.1 and 6.2 47% (80%) of the delayed onsets of the fluorescence are due to a deliberate switching of the DCP unit. Of course, it is not possible to assign "switching" and "blinking" to individual events.

6.2.4. The long-term Behaviour of the PPV

In order to test the long-term switching behaviour of the triads such experiments each consisting of 400 switching cycles and 400 control cycles were carried out repetitively, and the PPV was followed as a function of time. For the two triads used for Figures 6.1 and 6.2 the experiments were repeated 15 (PBI-DCP-PBI) and 11 (BODIPY-DCP-BODIPY) times and the result is shown in Figure 6.3. For both cases the PPVs feature narrow distributions characterized by 0.49 $\pm$ 0.05 (mean ± stdev) for PBI-DCP-PBI, and 0.79 $\pm$ 0.03 for BODIPY-DCP-BODIPY providing evidence of the high stability and fatigue resistance of the systems. In total we studied 20 individual triads of the PBI-DCP-PBI

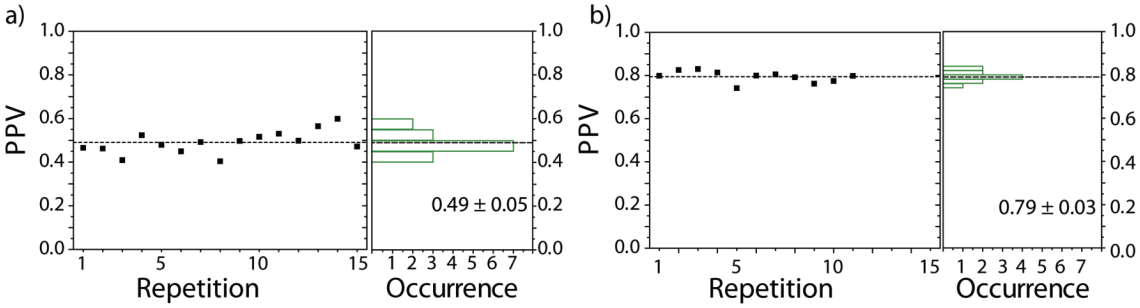

Figure 6.3.: *a) Positive predictive values (PPVs) for a single PBI-DCP-PBI triad obtained from 15 consecutively conducted experiments. The distribution of the PPV can be characterized by (mean* $\pm$ *stdev)* 0.49 ± 0.05 *b) Same as a) for 11 consecutively conducted experiments on a BODIPY-DCP-BOCIPY triad. The corresponding distribution can be characterized by* 0.79 ± 0.03*. Adapted from [135]*

type and 18 individual triads of the BODIPY-DCP-BODIPY type. For most of the other triads the experiments could be repeated 4 - 8 times corresponding to 1600 - 3200 cycles

or likewise to durations of 3200 s and 6400 s for the full experiments, respectively, before the fluorescence from the triads ceased. The distributions of the PPVs as a function of time, similar to those shown in Figure 6.3, featured mean values ranging from 0.49 - 0.86 for PBI-DCP-PBI (**Triad 2**) and 0.44 - 0.79 for BODIPY-DCP-BODIPY (**Triad 3**), with standard deviations between 0.01 and 0.08. Hence, for an individual triad the values of the PPVs were stable in time, whereas between individual triads large variations of this parameter can be observed. The resulting histograms of the mean values for the two types of triads are shown in Figure 6.4. The two distributions are similar within statistical error, and feature a mean of 0.7 ± 0.1. For PBI-DCP-PBI this is in line with results from Chapter 5, [106].

While the high fatigue resistance and an average PPV of 0.7 makes the tested triads

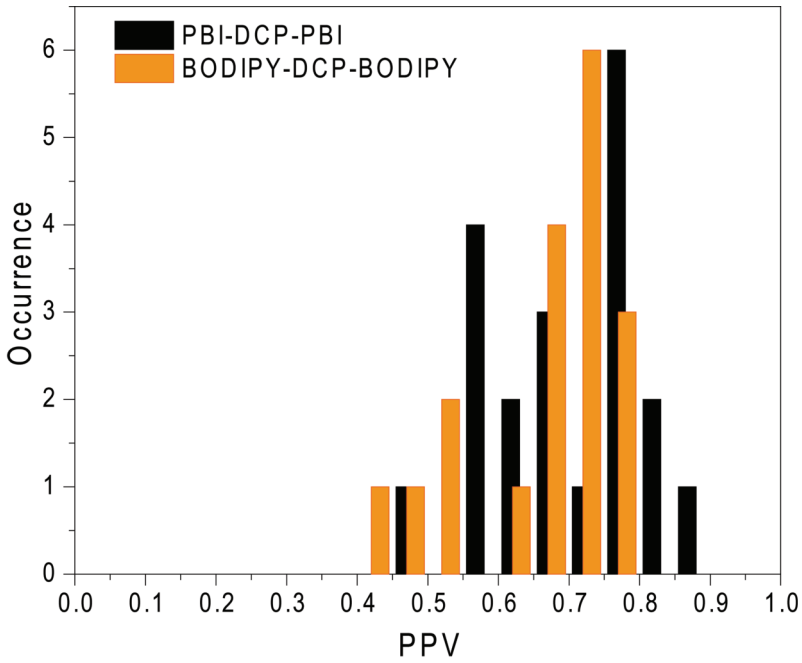

Figure 6.4.: *Distributions of the positive predictive values (PPVs) for 20 triads of PBI-DCP-PBI (black), and 18 triads of BODIPY-DCP-BODIPY (red). Both histograms can be characterized by* 0.7 ± 0.1 *(mean ± stdev). Adapted from [135]*

very suitable for super-resolution optical microscopy techniques that rely on the ON/OFF toggling of the emission of single molecules [4, 14, 15, 134, 136, 137], a PPV of 0.7 is far too low for optical data storage with single triads. However, an obvious question to ask is: How many triads would be required to exceed a predefined probabilty P that at least one of them has been switched? The probability that not a single triad out of n triads has been switched is given by

$$P(X=0) = \binom{n}{0} p^0 (1-p)^n = (1-p)^n, \tag{6.3}$$

where X refers to the number of triads that have been switched, and p corresponds to the PPV. Correspondingly $P(X \geq 1)$, i.e. the conditional probability that at least 1 out of n triads has been switched, is given by

$$P(X \geq 1) = 1 - P(X = 0) = 1 - (1 - p)^n, \tag{6.4}$$

and $P > P(X \geq 1)$ is fulfilled for

$$n > \frac{ln(1-P)}{ln(1-p)} \tag{6.5}$$

Table 6.1 summarizes some numerical values for n as a function of both the prescribed probability P and the average PPV. This shows that for a PPV of 0.7 as found in this work the value of $P > 1 - 10^{-6}$ (equivalent to a bit error ratio (BER) of 10^{-6}) is exceeded for $n = 12$. This raises the question whether it will be possible to distinguish the difference in

$P(X \geq 1)$	0.9	0.99	0.999	0.9999	$1 - 10^{-6}$
BER	10^{-1}	10^{-2}	10^{-3}	10^{-4}	10^{-6}
n; p = 0.7	**2**	**4**	**6**	**8**	**12**
n; p = 0.8	2	3	5	6	9
n; p = 0.9	1	2	3	4	6

Table 6.1.: *Number of triads, n, required to exceed a predefined probability $P(X \geq 1)$ that at least 1 triad out n triads has been switched for a given value p of the PPV. The bit error ratio (BER) is given as 1 - $P(X \geq 1)$). The line with bold letters refers to the PPV found in this work. Adapted from [135]*

the fluorescence signal if 1 triad out of 12 triads has been switched to the low-fluorescent state. In order to obtain a rough estimate of this, we consider a detection bandwidth of 100 Hz which is the inverse of the bin time of 10 ms used here for data acquisition. During this time interval we detect about 20 counts from a single triad. The change of the signal upon switching 1 out of 12 triads will be detectable as long as the noise of the signal from 12 triads does not exceed the signal from a single triad. Assuming shot noise only, the noise from 12 triads is 15 counts for the same detection bandwidth, which is just within the range to be detectable.

To summarize, under oxygen-free conditions the currently studied photochromic molecules based on DCP photoswitches can be reversibly interconverted between their bistable forms for several hundreds to thousands of cycles without detoriation. It can be verified at the single-molecule level that about 70% of the observed events are due to deliberate light-induced switching rather than stochastic blinking. Together with the high fatigue resistance this makes these systems well suited for super-resolution optical microscopy [4, 14, 15, 134, 136, 137]. However, the development of optical single-molecule memories using

these photochromic triads is far out of reach. Given the current PPV values, acceptable values for the error bit ratio in the order of 10^{-6} can only be achieved for small clusters of about 10 molecules. Within such a cluster the mutual distance between the individual triads should be large enough to suppress incoherent intermolecular energy transfer (FRET) [109, 110], which puts a lower limit on the possible miniaturization. A coarse estimate for the minimum dimensions of such a cluster is represented by a sphere with a radius in the order of the Förster radius of PBI, i.e. about 5 nm [34]. Still small in size, the preparation of such clusters with reproducible quality raises new problems concerning the assembly and positioning of such clusters. Unfortunately, a moderately increased PPV will not lead to a significant improvement of the situation as shown in Table 6.1.

7. Discussion and Summary

7.1. General Goal of the Dissertation project

This dissertation consists of two major fields of experiments. The goal of the research was to find an experimental way for the detection of switching events of single molecules with a home-built fluorescence microscope. For this purpose, considerations have been made in Chapters 3 and 4. In order to make the time until a switching of a photochromic triad takes place long enough for the detection on a time scale which is accessible in fluorescence microscopy, especially when speaking of a sampling time of 5 ms and10 ms, the switching process itself was artifically slowed down. The slowed reaction was achieved in two ways. The first way was the use of a photochromic triad which featured a larger distance between the molecular switch (DCP) and the fluorophore (PBI) compared to another, well-studied triad [21, 22, 25, 66] between this donor-acceptor pair. The synthesis of this triad with a second phenyl ring between DCP and PBI was done by the workgroup of Prof. Dr. Mukundan Thelakkat. The second way was the fact that the experiments were conducted at a low temperature of 10 K. From other studies [65, 66, 99, 101, 120] it is known that the cycloreversion reaction depends strongly on temperature, being slowed down upon decreasing temperature. To be precise, the cycloreversion efficiency of **Triad 1** drops to 0.7% of its room temperature value when cooling down to 10 K [66].
This led to the challenge of collecting enough signal from the single triads at low temperatures, which was achieved by integrating the SIL concept into the fluorescence microscope [67–69], thereby enhancing the collection efficiency and improving signal quality.
In other words, these considerations open the pathway for single molecule switching experiments.

7.2. Single Molecule Experiments on Photochromic Triads

Measurements on the change of fluorescence of single photochromic molecules due to the presence of UV light have already been made by Irie et al. and Fukaminato et al. [58, 59,

61], where the fluorescence transients of single photochromic molecules were measured in dependence of different UV illumination intensities. As a result, the distributions of "On"- and "Off"-times of the fluorescence transients of single photochromic molecules were presented, changing with the UV illumination intensities and the different matrices used for embedding the molecules. However, their expectation of an exponential distribution was not met by the gaussian distribution they found, leaving uncertain the influence of the blinking characteristics of single molecule emission.

In Chapter 5 (see also [106]), the above-mentioned measurement strategies were applied. Having shown in Chapter 3 that the cycloreversion reaction becomes slower upon reducing temperature, a first step to the detection of a single "On"-switching event was made: this way, the time until a triad switches, i. e. the time until fluorescence reappears, becomes longer, long enough for the detection with an avalanche photo diode (APD). As the APD measures with a binned time of 5 ms or 10 ms, the minimum for detectable switching times is 10 ms or 20 ms, respectively, representing twice the binned time. A second step was the introduction of triads with two phenyl rings between DCP and PBI instead of one, increasing the distance between the donor (PBI) and the acceptor (DCP) moiety (**Triad 2**, presented in Figure 3.3) As a consequence, energy transfer is reduced due to the longer distance between donor (PBI) and acceptor (DCP) [109, 110] and the switching rate is again lowered and the switching event itself, indicated by a delayed onset of fluorescence with respect to illumination, is further postponed. Nevertheless, a problem rises with the unavoidable blinking characteristics of the fluorescence of single molecules embedded in a polymer: one has to find a means to distinguish between an unwanted fluorescence delay caused by blinking, and a desired delay caused by deliberate switching [62, 63, 119]. For this reason, a statistical model was introduced, featuring conditional probabilities and the positive predictive value PPV as a probability to differentiate between switching and blinking in a statistical way. For one triad with 8800 switching cycles and 400 control cycles, a PPV of 0.7 was calculated. By analyzing experiments with the UV stimulus and comparing them with a control experiment, where the UV illumination was ceased, and an analysis of the telegraph-like "On"-/"Off"-blinking behaviour for 15 individual triads of the **Triad 2** species, an average PPV of 0.8 ± 0.1 was found. The application of the statistical methods and the introduction of the PPV is a powerful tool to distinguish between stochastic blinking and deliberate switching.

Concerning the deliberate switching of photochromic triads, additional measurements in dependence of the visible illumination intensity were done, showing only a weak variation of the PPV from 0.958 to 0.965 for varying the visible illumination intensity. Nevertheless, a triad was found here which showed a high PPV of 0.96, a value which is still not high enough for logical gating, but interesting for super-resolution imaging techniques like

PALM, STORM, RESOLFT or STED [5–9, 11, 136, 138]. An application in RESOLFT microscopy has already demonstrated an optical resolution of 75 nm with photochromic molecules [136]

In Chapter 6, experiments from Chapter 5 were first confirmed with the known DCP-PBI triad (**Triad 2**) and further enhanced by another type of triad. Instead of the PBI fluorophore moieties, this triad features BODIPY moieties as fluorophores (**Traid 3**), shown in Figure 3.4). Another feature with respect to Chapter 5 is the slightly changed concept of measurement. Having compared many switching experiments with one control experiment in Chapter 5, complete sets of measurements were done here, yielding one PPV for one measurement of 400 cycles with and 400 cycles without switching each. This allows for an observation of the PPV over long times, probing the fatigue resistance of the triads this way. On the average, 1600 - 3200 switching cycles could be repeated per triad, yielding 4 - 8 measurement repetitions and therefore PPVs per triad. The analysis showed an average PPV that varied in a wide range over the single triads measured, from 0.49 to 0.86 for **Triad 2** and 0.44 to 0.79 for **Triad 3**. Yet it remained stable within the measurements for each triad, showing only standard deviations between 0.01 and 0.08. Again, the PPV of one molecule itself is - on the average - too low for memory applications (0.7 ± 0.1 for both the 20 PBI-DCP-PBI and the 18 BODIPY-DCP-BODIPY triads measured), yet here, a model to enhance the probability for deliberate switching is presented. The model is based on the concept that if one triad alone only features a low PPV, a cluster of a small number of triads will still feature a telegraph-like switching of the fluorescence signal if at least one triad switches (for larger numbers of triads, i. e. ensembles, one expects the switching curves described in Chapter 3.6.1 again). Applying this model, an ensemble of only 12 triads with a PPV of 0.7 for the switching of a single triad can enhance the probability to 0.999999 or, seen from the electronics point of view, the bit-error-ratio is reduced to $1 - 0.999999 = 10^{-6}$, still being visible in the fluorescence signal as an additional digital jump to a higher or lower level. Based on this, the triads can become promising molecules for memory application, as they are smaller than current silicon technologies, given that such a cluster can be assembled and positioned in a way that they can be read out as one "bit".

This dissertation shows that it is possible to access the switching of single photochromic triads experimentally on a millisecond timescale with fluorescence microscopy, and to sort out the influence of blinking, which obscures the deliberate switching signal, in a statistical way. This was done in oxygen-free, low temperature conditions for many switching cycles of single triads.

References

[1] H. Dürr and H. Bouas-Laurent, eds. *Photochromism: Molecules and Systems*. *Studies in organic chemistry*. Amsterdam: Elsevier Science, 1990.

[2] Ben L. Feringa and Wesley R. Browne, eds. *Molecular Switches*. Wiley-VCH Verlag GmbH & Co. KGaA, 2011.

[3] Mike Heilemann, Peter Dedecker, Johan Hofkens and Markus Sauer. *Photoswitches: Key molecules for subdiffraction-resolution fluorescence imaging and molecular quantification*. Laser and Photonics Reviews 3 (2009), 180–202.

[4] Oleksii Nevskyi, Dmytro Sysoiev, Jes Dreier, Simon Christoph Stein, Alex Oppermann, Florian Lemken, Tobias Janke, Jörg Enderlein, Ilaria Testa, Thomas Huhn and Dominik Wöll. *Fluorescent Diarylethene Photoswitches-A Universal Tool for Super-Resolution Microscopy in Nanostructured Materials*. Small 14 (2018), 1703333.

[5] Michael J Rust, Mark Bates and Xiaowei Zhuang. *Sub-diffraction-limit imaging by stochastic optical reconstruction microscopy (STORM)*. Nature Methods 3 (2006), 793–796.

[6] E. Betzig, G. H. Patterson, R. Sougrat, O. W. Lindwasser, S. Olenych, J. S. Bonifacino, M. W. Davidson, J. Lippincott-Schwartz and H. F. Hess. *Imaging Intracellular Fluorescent Proteins at Nanometer Resolution*. Science 313 (2006), 1642–1645.

[7] Stefan W. Hell and Jan Wichmann. *Breaking the diffraction resolution limit by stimulated emission: stimulated-emission-depletion fluorescence microscopy*. Optics Letters 19 (1994), 780.

[8] Mariano Bossi, Vladimir Belov, Svetlana Polyakova and Stefan W. Hell. *Reversible red fluorescent molecular switches*. Angewandte Chemie - International Edition 45 (2006), 7462–7465. arXiv: 1408.1149.

[9] Mariano Bossi, Jonas Fölling, Marcus Dyba, Volker Westphal and Stefan W. Hell. *Breaking the diffraction resolution barrier in far-field microscopy by molecular optical bistability*. New Journal of Physics 8 (2006).

[10] S. W. Hell and M. Kroug. *Ground-state-depletion fluorscence microscopy: A concept for breaking the diffraction resolution limit*. Applied Physics B Lasers and Optics 60 (1995), 495–497.

[11] Jan Vogelsang, Thorben Cordes, Carsten Forthmann, Christian Steinhauer and Philip Tinnefeld. *Intrinsically resolution enhancing probes for confocal microscopy*. Nano Letters 10 (2010), 672–679.

[12] Francisco Balzarotti, Yvan Eilers, Klaus C. Gwosch, Arvid H. Gynnå, Volker Westphal, Fernando D. Stefani, Johan Elf and Stefan W. Hell. *Nanometer resolution imaging and tracking of fluorescent molecules with minimal photon fluxes*. Science 355 (2017), 606–612.

[13] C. Bertarelli, A. Bianco, R. Castagna and G. Pariani. *Photochromism into optics: Opportunities to develop light-triggered optical elements*. Journal of Photochemistry and Photobiology C: Photochemistry Reviews 12 (2011), 106–125.

[14] Dominik Wöll and Cristina Flors. *Super-resolution Fluorescence Imaging for Materials Science*. Small Methods 1 (2017), 1700191.

[15] Benoit Roubinet, Michael Weber, Heydar Shojaei, Mark Bates, Mariano L. Bossi, Vladimir N. Belov, Masahiro Irie and Stefan W. Hell. *Fluorescent Photoswitchable Diarylethenes for Biolabeling and Single-Molecule Localization Microscopies with Optical Superresolution*. Journal of the American Chemical Society 139 (2017), 6611–6620.

[16] Eric Betzig. *Single Molecules, Cells, and Super-Resolution Optics (Nobel Lecture)*. Angewandte Chemie - International Edition 54 (2015), 8034–8053.

[17] Stefan W. Hell. *Nanoscopy with Focused Light (Nobel Lecture)*. Angewandte Chemie International Edition 54 (2015), 8054–8066.

[18] William E. Moerner. *Single-Molecule Spectroscopy, Imaging, and Photocontrol: Foundations for Super-Resolution Microscopy (Nobel Lecture)*. Angewandte Chemie - International Edition 54 (2015), 8067–8093.

[19] Samsung Press Release. https://news.samsung.com/global/samsung-electronics-starts-production-of-euv-based-7nm-lpp-process. 2018.

[20] Masahiro Irie, Tuyoshi Fukaminato, Kenji Matsuda and Seiya Kobatake. *Photochromism of diarylethene molecules and crystals: memories, switches, and actuators.* Chemical reviews 114 (2014), 12174–277.

[21] Martti Pärs, Christiane C. Hofmann, Katja Willinger, Peter Bauer, Mukundan Thelakkat and Jürgen Köhler. *An organic optical transistor operated under ambient conditions*. Angewandte Chemie - International Edition 50 (2011), 11405–11408.

[22] Martti Pärs, Katja Gräf, Peter Bauer, Mukundan Thelakkat and Jürgen Köhler. *Optical gating of perylene bisimide fluorescence using dithienylcyclopentene photochromic switches*. Applied Physics Letters 103 (2013), 221115.

[23] Jia Su, Tuyoshi Fukaminato, Jean Pierre Placial, Tsunenobu Onodera, Ryuju Suzuki, Hidetoshi Oikawa, Arnaud Brosseau, François Brisset, Robert Pansu, Keitaro Nakatani and Rémi Métivier. *Giant Amplification of Photoswitching by a Few Photons in Fluorescent Photochromic Organic Nanoparticles*. Angewandte Chemie - International Edition 55 (2016), 3662–3666.

[24] Emanuele Orgiu, Núria Crivillers, Martin Herder, Lutz Grubert, Michael Pätzel, Johannes Frisch, Egon Pavlica, Duc T. Duong, Gvido Bratina, Alberto Salleo, Norbert Koch, Stefan Hecht and Paolo Samorì. *Optically switchable transistor via energy-level phototuning in a bicomponent organic semiconductor*. Nature Chemistry 4 (2012), 675–679.

[25] Martti Pärs, Michael Gradmann, Katja Gräf, Peter Bauer, Mukundan Thelakkat and Jürgen Köhler. *Optical gating with organic building blocks. A quantitative model for the fluorescence modulation of photochromic perylene bisimide dithienylcyclopentene triads.* Scientific reports 4 (2014), 4316.

[26] Satyaprasad P. Senanayak, Vinod K. Sangwan, Julian J. McMorrow, Ken Everaerts, Zhihua Chen, Antonio Facchetti, Mark C. Hersam, Tobin J. Marks and K. S. Narayan. *Self-Assembled Photochromic Molecular Dipoles for High-Performance Polymer Thin-Film Transistors*. ACS Applied Materials and Interfaces 10 (2018), 21492–21498.

[27] Mirella El Gemayel, Karl Börjesson, Martin Herder, Duc T. Duong, James A. Hutchison, Christian Ruzié, Guillaume Schweicher, Alberto Salleo, Yves Geerts, Stefan Hecht, Emanuele Orgiu and Paolo Samorì. *Optically switchable transistors by simple incorporation of photochromic systems into small-molecule semiconducting matrices*. Nature Communications 6 (2015), 1–8.

[28] Joakim Andréasson and Uwe Pischel. *Smart molecules at work—mimicking advanced logic operations*. Chem. Soc. Rev. 39 (2010), 174–188.

[29] Joakim Andréasson and Uwe Pischel. *Molecules with a sense of logic: a progress report.* Chemical Society reviews 44 (2015), 1053–69.

[30] Emanuele Orgiu and Paolo Samorì. *25Th Anniversary Article: Organic Electronics Marries Photochromism: Generation of Multifunctional Interfaces, Materials, and Devices.* Advanced materials (Deerfield Beach, Fla.) 26 (2014), 1827–45.

[31] Davood Taherinia and C. Daniel Frisbie. *Photoswitchable Hopping Transport in Molecular Wires 4 nm in Length*. The Journal of Physical Chemistry C 120 (2016), 6442–6449.

[32] Taichi Toyama, Kenji Higashiguchi, Tsukuru Nakamura, Hidehiro Yamaguchi, Eriko Kusaka and Kenji Matsuda. *Photoswitching of Conductance of Diarylethene-Gold Nanoparticle Network Based on the Alteration of π-Conjugation*. Journal of Physical Chemistry Letters 7 (2016), 2113–2118.

[33] Christian Schörner, Daniela Wolf, Thorsten Schumacher, Peter Bauer, Mukundan Thelakkat and Markus Lippitz. *Nondestructive Probing of a Photoswitchable Dithienylethene Coupled to Plasmonic Nanostructures*. Journal of Physical Chemistry C 121 (2017), 16528–16532.

[34] R. Schmidt, M. Pärs, T. Weller, M. Thelakkat and J. Köhler. *Trapping on demand: External regulation of excitation energy transfer in a photoswitchable smart matrix*. Applied Physics Letters 104 (2014), 4–7.

[35] D. A. Parthenopoulos and P. M. Rentzepis. *Three-Dimensional Optical Storage Memory*. Science 245 (1989), 843–845.

[36] Masahiro Irie. *Diarylethenes for Memories and Switches*. Chemical Reviews 100 (2000), 1685–1716.

[37] Giorgio Pariani, Rossella Castagna, Giovanni Dassa, Stephan Hermes, Claudio Vailati, Andrea Bianco and Chiara Bertarelli. *Diarylethene-based photochromic polyurethanes for multistate optical memories*. Journal of Materials Chemistry 21 (2011), 13223.

[38] Guiyuan Jiang, Sheng Wang, Wenfang Yuan, Lei Jiang, Yanlin Song, He Tian and Daoben Zhu. *Highly Fluorescent Contrast for Rewritable Optical Storage Based on Photochromic Bisthienylethene-Bridged Naphthalimide Dimer*. Chemistry of Materials 18 (2006), 235–237.

[39] Kesar Tandekar, Somenath Garai and Sabbani Supriya. *A Reversible Redox Reaction in a Keggin Polyoxometalate Crystal Driven by Visible Light: A Programmable Solid-State Photochromic Switch*. Chemistry - A European Journal 24 (2018), 9747–9753.

[40] Martin Berberich, Ana Maria Krause, Michele Orlandi, Franco Scandola and Frank Würthner. *Toward fluorescent memories with nondestructive readout: Photoswitching of fluorescence by intramolecular electron transfer in a diaryl ethene-perylene bisimide photochromic system*. Angewandte Chemie - International Edition 47 (2008), 6616–6619.

[41] Na Zhang, Wai-Yip Lo, Anex Jose, Zhengxu Cai, Lianwei Li and Luping Yu. *A Single-Molecular AND Gate Operated with Two Orthogonal Switching Mechanisms*. Advanced Materials 29 (2017), 1701248.

[42] Gaowa Naren, Shiming Li and Joakim Andréasson. *One-Time Password Generation and Two-Factor Authentication Using Molecules and Light*. ChemPhysChem 18 (2017), 1726–1729.

[43] Ambra Dreos, Zhihang Wang, Behabitu E. Tebikachew, Kasper Moth-Poulsen and Joakim Andréasson. *Three-Input Molecular Keypad Lock Based on a Norbornadiene–Quadricyclane Photoswitch*. The Journal of Physical Chemistry Letters 9 (2018), 6174–6178.

[44] Tianyou Qin, Jiaqi Han, Yue Geng, Le Ju, Lan Sheng and Sean Xiao An Zhang. *A Multiaddressable Dyad with Switchable Cyan/Magenta/Yellow Colors for Full-Color Rewritable Paper*. Chemistry - A European Journal 24 (2018), 12539–12545.

[45] Kunihiro Ichimura, Yasuzo Suzuki, Takahiro Seki, Akira Hosoki and Koso Aoki. *Reversible change in alignment mode of nematic liquid crystals regulated photochemically by "command surfaces" modified with an azobenzene monolayer*. Langmuir 4 (1988), 1214–1216.

[46] Chagit Denekamp and Ben L Feringa. *Optically Active Diarilethenes for Multimode Photoswitching Between Liquid-Crysalline Phases*. Advanced Materials 10 (1998), 1080–1082.

[47] P. Zhang, E. Buncel and R. P. Lemieux. *Compatibilization of a Photochromic Dithienylethene Dopant and Ferroelectric Liquid-Crystal Host via Siloxane Nanosegregation*. Advanced Materials 17 (2005), 567–571.

[48] Masahiro Irie, Thorsten Lifka, Seiya Kobatake and Nobuo Kato. *Photochromism of 1, 2-Bis(2-methyl-5-phenyl-3-thienyl)perfluorocyclopentene in a Single-Crystalline Phase*. Journal of the American Chemical Society 122 (2000), 4871–4876.

[49] M. Irie. *Reversible Surface Morphology Changes of a Photochromic Diarylethene Single Crystal by Photoirradiation*. Science 291 (2001), 1769–1772.

[50] Nagatoshi Koumura, Robert W. J. Zijlstra, Richard A. van Delden, Nobuyuki Harada and Ben L. Feringa. *Light-driven monodirectional molecular rotor*. Nature 401 (1999), 152–155.

[51] Tibor Kudernac, Nopporn Ruangsupapichat, Manfred Parschau, Beatriz Maciá, Nathalie Katsonis, Syuzanna R. Harutyunyan, Karl-Heinz Ernst and Ben L. Feringa. *Electrically driven directional motion of a four-wheeled molecule on a metal surface*. Nature 479 (2011), 208–211.

[52] Beatrice S. L. Collins, Jos C. M. Kistemaker, Edwin Otten and Ben L. Feringa. *A chemically powered unidirectional rotary molecular motor based on a palladium redox cycle*. Nature Chemistry 8 (2016), 860–866.

[53] Jean-Pierre Sauvage. *From Chemical Topology to Molecular Machines (Nobel Lecture)*. Angewandte Chemie International Edition 56 (2017), 11080–11093.

[54] J. Fraser Stoddart. *Mechanically Interlocked Molecules (MIMs)-Molecular Shuttles, Switches, and Machines (Nobel Lecture)*. Angewandte Chemie International Edition 56 (2017), 11094–11125.

[55] Ben L. Feringa. *The Art of Building Small: From Molecular Switches to Motors (Nobel Lecture)*. Angewandte Chemie International Edition 56 (2017), 11060–11078.

[56] Herbert Paschen, Christopher Coenen, Torsten Fleischer, Reinhard Grünwald, Dagmar Oertel and Christoph Revermann. *TA-Projekt Nanotechnologie - Endbericht*. Büro für Technikfolgenabschätzung des Deutschen Bundestages Bonn, 2003.

[57] Tuyoshi Fukaminato. *Single-molecule fluorescence photoswitching: Design and synthesis of photoswitchable fluorescent molecules*. Journal of Photochemistry and Photobiology C: Photochemistry Reviews 12 (2011), 177–208.

[58] Masahiro Irie. *A digital fluorescent molecular photoswitch*. Nature 420 (2002), 759–760.

[59] Tuyoshi Fukaminato, Takatoshi Sasaki, Tsuyoshi Kawai, Naoto Tamai and Masahiro Irie. *Digital photoswitching of fluorescence based on the photochromism of diarylethene derivatives at a single-molecule level.* Journal of the American Chemical Society 126 (2004), 14843–9.

[60] Tuyoshi Fukaminato, Takao Doi, Nobuyuki Tamaoki, Katsuki Okuno, Yukihide Ishibashi, Hiroshi Miyasaka and Masahiro Irie. *Single-molecule fluorescence photoswitching of a diarylethene- perylenebisimide dyad: Non-destructive fluorescence readout*. Journal of the American Chemical Society 133 (2011), 4984–4990.

[61] Tuyoshi Fukaminato, Tohru Umemoto, Yasuhide Iwata, Satoshi Yokojima, Mitsuru Yoneyama, Shinichiro Nakamura and Masahiro Irie. *Photochromism of diarylethene single molecules in polymer matrices*. Journal of the American Chemical Society 129 (2007), 5932–5938.

[62] F. Cichos, C. von Borczyskowski and M. Orrit. *Power-law intermittency of single emitters*. Current Opinion in Colloid and Interface Science 12 (2007), 272–284.

[63] Markus Lippitz, Florian Kulzer and Michel Orrit. *Statistical evaluation of single nano-object fluorescence*. ChemPhysChem 6 (2005), 770–789.

[64] Sebastian van de Linde and Markus Sauer. *How to switch a fluorophore: from undesired blinking to controlled photoswitching.* Chemical Society reviews 43 (2014), 1076–87.

[65] Johann Thurn. *Spektroskopische Charakterisierung der Temperaturabhängigkeit des Schaltverhaltens photochromer Triaden, Master Thesis*. Universität Bayreuth, 2014.

[66] Johann Thurn, Johannes Maier, Martti Pärs, Katja Gräf, Mukundan Thelakkat and Jürgen Köhler. *Temperature dependence of the conversion efficiency of photochromic perylene bisimide dithienylcyclopentene triads embedded in a polymer*. Physical Chemistry Chemical Physics 19 (2017), 26065–26071.

[67] S. M. Mansfield and G. S. Kino. *Solid immersion microscope*. Applied Physics Letters 57 (1990), 2615–2616.

[68] Holger Gilbergs. *Entwicklung eines Immersionsobjektives, Diplomarbeit*. Universität Bayreuth, 2008.

[69] Johannes Maier. *Einzelmolekül-Imaging bei tiefen Temperaturen mit Hilfe eines Festkörper-Immersionsobjektives, Master Thesis*. Universität Bayreuth, 2015.

[70] G. H. Brown, ed. *Photochromism*. New York: Wiley, 1971.

[71] 'Molecular and Supramolecular Devices'. *Supramolecular Chemistry*. Wiley-VCH Verlag GmbH & Co. KGaA, 2006, 89–138.

[72] M. Irie, Y. Yokoyama and T. Seki, eds. *New Frontiers in Photochromism*. Springer Japan, 2013.

[73] Jesse H. Day. *Thermochromism.* Chemical Reviews 63 (1963), 65–80.

[74] Alberto Marini, Aurora Munoz-Losa, Alessandro Biancardi and Benedetta Mennucci. *What is Solvatochromism?* The Journal of Physical Chemistry B 114 (2010), 17128–17135.

[75] Ralf Giernoth. *Solvents and Solvent Effects in Organic Chemistry. 4th Ed. By Christian Reichardt and Thomas Welton.* Angewandte Chemie International Edition 50 (2011), 11289–11289.

[76] Bernd Speiser. *Electrochromism. Fundamentals and applications. VonP. M. S. Monk, R. J. Mortimer und D. R. Rosseinsky. VCH Verlagsgesellschaft, Weinheim, 1995.* Angewandte Chemie 108 (1996), 853–854.

[77] M. Fritzsche. *Note sur les carbures d'hydrogène solides, tirés du goudron de houille*. Comptes Rendus de l'Academie des Sciences 69 (1867), 1035–1037.

[78] Edm. ter Meer. *Ueber Dinitroverbindungen der Fettreihe*. Justus Liebig's Annalen der Chemie 181 (1876), 1–22.

[79] W. Marckwald. *Ueber Phototropie*. Zeitschrift für Physikalische Chemie 30U (1899).

[80] L. v. Mechel and H. Stauffer. *Zur Kenntnis der phototropen Aminoazofarbstoffe*. Helvetica Chimica Acta 24 (1941), 151E–161E.

[81] Yehuda M. Hirshberg. *Photochromie dans la serie de la bianthrone. Band 231, Nr. 903, 1950*. Comptes Rendus de l'Academie des Sciences 231 (1950), 903.

[82] Yehuda Hirshberg and Ernst Fischer. *Photochromism and reversible multiple internal transitions in some spiropyrans at low temperatures. Part I*. Journal of the Chemical Society (Resumed) (1954), 297.

[83] Yehuda Hirshberg. *Reversible Formation and Eradication of Colors by Irradiation at Low Temperatures. A Photochemical Memory Model*. Journal of the American Chemical Society 78 (1956), 2304–2312.

[84] Masahiro Irie and Masaaki Mohri. *Thermally irreversible photochromic systems. Reversible photocyclization of diarylethene derivatives*. The Journal of Organic Chemistry 53 (1988), 803–808.

[85] Masahiro Irie and Kingo Uchida. *Synthesis and Properties of Photochromic Diarylethenes with Heterocyclic Aryl Groups*. Bulletin of the Chemical Society of Japan 71 (1998), 985–996.

[86] Heinz Dürr. *Organische Photochromie*. Angewandte Chemie 116 (2004), 3404–3418.

[87] Masahiro Irie and Masakazu Morimoto. *Photoswitchable Turn-on Mode Fluorescent Diarylethenes: Strategies for Controlling the Switching Response*. Bulletin of the Chemical Society of Japan 91 (2018), 237–250.

[88] Masahiro Irie, Tuyoshi Fukaminato, Kenji Matsuda and Seiya Kobatake. *Photochromism of diarylethene molecules and crystals: Memories, switches, and actuators*. Chemical Reviews 114 (2014), 12174–12277.

[89] G. S. HARTLEY. *The Cis-form of Azobenzene*. Nature 140 (1937), 281–281.

[90] David H. Waldeck. *Photoisomerization dynamics of stilbenes*. Chemical Reviews 91 (1991), 415–436.

[91] Roseanne J. Sension, Stephen T. Repinec, Arpad Z. Szarka and Robin M. Hochstrasser. *Femtosecond laser studies of the cis-stilbene photoisomerization reactions*. The Journal of Chemical Physics 98 (1993), 6291–6315.

[92] Frank B. Mallory and Clelia W. Mallory. 'Photocyclization of Stilbenes and Related Molecules'. *Organic Reactions*. American Cancer Society, 2005. Chap. 1, 1–456.

[93] Luuk Kortekaas and Wesley R. Browne. *The evolution of spiropyran: fundamentals and progress of an extraordinarily versatile photochrome*. Chemical Society Reviews 48 (2019), 3406–3424.

[94] Martin Handschuh, Martin Seibold, Helmut Port and Hans Christoph Wolf. *Dynamics of the cyclization reaction in photochromic furyl fulgides*. Journal of Physical Chemistry A 101 (1997), 502–506.

[95] Thomas Brust, Simone Draxler, Jonas Eicher, Watson J. Lees, Karola Rück-Braun, Wolfgang Zinth and Markus Braun. *Increasing the efficiency of the ring-opening reaction of photochromic indolylfulgides by optical pre-excitation*. Chemical Physics Letters 489 (2010), 175–180. arXiv: NIHMS150003.

[96] Shinichiro Nakamura and Masahiro Irie. *Thermally irreversible photochromic systems. A theoretical study*. The Journal of Organic Chemistry 53 (1988), 6136–6138.

[97] Makoto Hanazawa, Ritsuo Sumiya, Yukio Horikawa and Masahiro Irie. *Thermally irreversible photochromic systems. Reversible photocyclization of 1, 2-bis (2-methylbenzo[b]thiophen-3-yl)perfluorocyclocoalkene derivatives*. Journal of the Chemical Society, Chemical Communications (1992), 206.

[98] John H. Frederick, Y. Fujiwara, John H. Penn, Keitaro Yoshihara and Hrvoje Petek. *Models for stilbene photoisomerization: experimental and theoretical studies of the excited-state dynamics of 1, 2-diphenylcycloalkenes*. The Journal of Physical Chemistry 95 (1991), 2845–2858.

[99] Martial Boggio-Pasqua, Marcella Ravaglia, Michael J. Bearpark, Marco Garavelli and Michael A. Robb. *Can Diarylethene Photochromism Be Explained by a Reaction Path Alone? A CASSCF Study with Model MMVB Dynamics*. The Journal of Physical Chemistry A 107 (2003), 11139–11152.

[100] Na Xin, Chuancheng Jia, Jinying Wang, Shuopei Wang, Mingliang Li, Yao Gong, Guangyu Zhang, Daoben Zhu and Xuefeng Guo. *Thermally Activated Tunneling Transition in a Photoswitchable Single-Molecule Electrical Junction*. The Journal of Physical Chemistry Letters 8 (2017), 2849–2854.

[101] Tibor Kudernac, Takao Kobayashi, Ayaka Uyama, Kingo Uchida, Shinichiro Nakamura and Ben L. Feringa. *Tuning the temperature dependence for switching in dithienylethene photochromic switches*. Journal of Physical Chemistry A 117 (2013), 8222–8229.

[102] Jan Ern, Arthur T. Bens, Hans-Dieter Martin, Karla Kuldova, H. Peter Trommsdorff and Carola Kryschi. *Ring-Opening and -Closure Reaction Dynamics of a Photochromic Dithienylethene Derivative*. The Journal of Physical Chemistry A 106 (2002), 1654–1660.

[103] Sangdeok Shim, Intae Eom, Taiha Joo, Eunkyoung Kim and Kwang S. Kim. *Ring closure reaction dynamics of diarylethene derivatives in solution*. Journal of Physical Chemistry A 111 (2007), 8910–8917.

[104] Maolin Yu, Peisheng Zhang, Baiju P. Krishnan, Hong Wang, Yong Gao, Shu Chen, Rongjin Zeng, Jiaxi Cui and Jian Chen. *From a Molecular Toolbox to a Toolbox for Photoswitchable Fluorescent Polymeric Nanoparticles*. Advanced Functional Materials 28 (2018), 1–11.

[105] Tsuyoshi Kawai, Myeong-Suk Kim, Takatoshi Sasaki and Masahiro Irie. *Fluorescence switching of photochromic diarylethenes*. Optical Materials 21 (2003), 275–278.

[106] Johannes Maier, Martti Pärs, Tina Weller, Mukundan Thelakkat and Jürgen Köhler. *Deliberate Switching of Single Photochromic Triads*. Scientific Reports 7 (2017), 41739.

[107] Chuang Zhang, Yongli Yan, Yong Sheng Zhao and Jiannian Yao. *From Molecular Design and Materials Construction to Organic Nanophotonic Devices*. Accounts of Chemical Research 47 (2014), 3448–3458.

[108] Ying Ma, Boxing An, Meng Wang, Fangxiao Shi, Qing Wang, Yaxin Gu, Wanyang Niu, Zhaorong Fan, Yanli Shang, Dan Wang and Cong Zhao. *The controllable assembly of nanorods, nanowires and microwires of a perylenediimide molecule with photoswitching property*. Journal of Solid State Chemistry 227 (2015), 219–222.

[109] Th. Förster and Th. Forster. *Transfer Mechanisms of Electronic Excitation Energy*. Radiation Research Supplement 2 (1960), 326.

[110] Alexandra Olaya-Castro and Gregory D. Scholes. *Energy transfer from Förster–Dexter theory to quantum coherent light-harvesting*. International Reviews in Physical Chemistry 30 (2011), 49–77.

[111] Martti Pärs. Implementation of the LabView and ADbasic program for the control of the measurement setup. 2014.

[112] Frank Würthner. *Perylene bisimide dyes as versatile building blocks for functional supramolecular architectures*. Chem. Commun. (2004), 1564–1579. arXiv: 0903.1670.

[113] Tanja Weil, Tom Vosch, Johan Hofkens, Kalina Peneva and Klaus Müllen. *The rylene colorant family–tailored nanoemitters for photonics research and applications.* Angewandte Chemie (International ed. in English) 49 (2010), 9068–93.

[114] Erwin Lang, Richard Hildner, Hanna Engelke, Peter Osswald, Frank Würthner and Jürgen Köhler. *Comparison of the photophysical parameters for three perylene bisimide derivatives by single-molecule spectroscopy*. ChemPhysChem 8 (2007), 1487–1496.

[115] Xiaowei Zhan, Antonio Facchetti, Stephen Barlow, Tobin J. Marks, Mark A. Ratner, Michael R. Wasielewski and Seth R. Marder. *Rylene and related diimides for organic electronics*. Advanced Materials 23 (2011), 268–284.

[116] Alfred Treibs and Franz-Heinrich Kreuzer. *Difluorboryl-Komplexe von Di- und Tripyrrylmethenen*. Justus Liebigs Annalen der Chemie 718 (1968), 208–223.

[117] Aurore Loudet and Kevin Burgess. *BODIPY Dyes and Their Derivatives: Syntheses and Spectroscopic Properties*. Chemical Reviews 107 (2007), 4891–4932.

[118] M. Nirmal, B. O. Dabbousi, M. G. Bawendi, J. J. Macklin, J. K. Trautman, T. D. Harris and L. E. Brus. *Fluorescence intermittency in single cadmium selenide nanocrystals*. Nature 383 (1996), 802–804.

[119] Edwin K. L. Yeow, Sergey M. Melnikov, Toby D. M. Bell, Frans C. De Schryver and Johan Hofkens. *Characterizing the Fluorescence Intermittency and Photobleaching Kinetics of Dye Molecules Immobilized on a Glass Surface*. The Journal of Physical Chemistry A 110 (2006), 1726–1734.

[120] D. Dulić, T. Kudernac, A. Pužys, B. L. Feringa and B. J. van Wees. *Temperature Gating of the Ring-Opening Process in Diarylethene Molecular Switches*. Advanced Materials 19 (2007), 2898–2902. eprint: `https://onlinelibrary.wiley.com/doi/pdf/10.1002/adma.200700161`.

[121] Mounir Maafi and Robert G. Brown. *The kinetic model for AB(1ϕ{symbol}) systems. A closed-form integration of the differential equation with a variable photokinetic factor*. Journal of Photochemistry and Photobiology A: Chemistry 187 (2007), 319–324.

[122] J. Sworakowski, K. Janus and S. Nešpůrek. *Kinetics of photochromic reactions in condensed phases*. Advances in Colloid and Interface Science 116 (2005), 97–110.

[123] S. M. Ross. *Stochastic Processes*. 2nd ed. New York: Wiley, 1996.

[124] E. Hecht. *Optik*. 6th ed. *De Gruyter Studium*. De Gruyter, 2014.

[125] G.S. Kino and T.R. Corle. *Confocal Scanning Optical Microscopy and Related Imaging Systems*. Elsevier Science, 1996.

[126] J. B. Pawley, ed. *Handbook of Biological Confocal Microscopy*. 2nd ed. New York: Plenum Press, 1995.

[127] Jan Jasny, Jerzy Sepiol, Thomas Irngartinger, Markus Traber, Alois Renn and Urs P. Wild. *Fluorescence microscopy in superfluid helium: Single molecule imaging*. Review of Scientific Instruments 67 (1996), 1425–1430.

[128] Kazuko Koyama, Masahiro Yoshita, Motoyoshi Baba, Tohru Suemoto and Hidefumi Akiyama. *High collection efficiency in fluorescence microscopy with a solid immersion lens*. Applied Physics Letters 75 (1999), 1667–1669.

[129] K. Karrai, X. Lorenz and L. Novotny. *Enhanced reflectivity contrast in confocal solid immersion lens microscopy*. Applied Physics Letters 77 (2000), 3459–3461.

[130] Masahiro Yoshita, Kazuko Koyama, Yuhei Hayamizu, Motoyoshi Baba and Hidefumi Akiyama. *Improved High Collection Efficiency in Fluorescence Microscopy with a Weierstrass-Sphere Solid Immersion Lens*. Japanese Journal of Applied Physics 41 (2002), L858–L860.

[131] Arash Darafsheh, Nicholaos I. Limberopoulos, John S. Derov, Dennis E. Walker and Vasily N. Astratov. *Advantages of microsphere-assisted super-resolution imaging technique over solid immersion lens and confocal microscopies*. Applied Physics Letters 104 (2014).

[132] Edward H. Hellen and Daniel Axelrod. *Fluorescence emission at dielectric and metal-film interfaces*. Journal of the Optical Society of America B 4 (1987), 337.

[133] Karl Bosch. *Elementare Einführung in die Wahrscheinlichkeitsrechnung*. 11th ed. Wiesbaden: Vieweg und Teubner, 2011.

[134] Oleksii Nevskyi, Dmytro Sysoiev, Alex Oppermann, Thomas Huhn and Dominik Wöll. *Nanoscopic Visualization of Soft Matter Using Fluorescent Diarylethene Photoswitches*. Angewandte Chemie - International Edition 55 (2016), 12698–12702.

[135] Johannes Maier, Tina Weller, Mukundan Thelakkat and Jürgen Köhler. *Long-term switching of single photochromic triads based on dithienylcyclopentene and fluorophores at cryogenic temperatures*. The Journal of Chemical Physics 155 (2021), 014901.

[136] Benoît Roubinet, Mariano L. Bossi, Philipp Alt, Marcel Leutenegger, Heydar Shojaei, Sebastian Schnorrenberg, Shamil Nizamov, Masahiro Irie, Vladimir N. Belov and Stefan W. Hell. *Carboxylated Photoswitchable Diarylethenes for Biolabeling and Super-Resolution RESOLFT Microscopy*. Angewandte Chemie - International Edition 55 (2016), 15429–15433.

[137] Benoît Roubinet, Mariano L. Bossi, Philipp Alt, Marcel Leutenegger, Heydar Shojaei, Sebastian Schnorrenberg, Shamil Nizamov, Masahiro Irie, Vladimir N. Belov and Stefan W. Hell. *Carboxylierte photoschaltbare Diarylethene als Biomarkierungen für hochauflösende RESOLFT-Mikroskopie*. Angewandte Chemie 128 (2016), 15655–15659.

[138] Jiwoong Kwon, Jihee Hwang, Jaewan Park, Gi Rim Han, Kyu Young Han and Seong Keun Kim. *RESOLFT nanoscopy with photoswitchable organic fluorophores*. Scientific Reports 5 (2015), 1–8.

A. Materials and Equipment

A.1. Chemicals

Table A.1 gives an overview over the chemicals used during sample preparation.

Trade name	chemical name	Manufacturer
PMMA	Poly(methyl methacrylate) PDI = 1.05, $M_p = 9680$, $M_w = 9590$, $M_n = 9100$	PSS - Polymer Standards Services
PS	Polystyrene PDI = 1.08, $Mw = 1010$	PSS - Polymer Standards Services
Chloroform	Trichloromethane Purity $> 99.9\%$	Sigma Aldrich
Toluene	Methylbenzene Purity $> 99.7\%$	Sigma Aldrich

Table A.1.: *The chemicals used for sample preparation and their manufacturers.*

A.2. Equipment

In Table A.2, the tools and devices used for measurements and sample preparation are listed.

A.3. Optical Components

Table A.3 summarizes the main optical components used in the experimental setup.

Device	Type	Manufacturer
Spin coater	P6700	Specialty Coating Systems
UV-Laser	IK Series HeCd-Laser IK3201R-F	Kimmon
Probe Laser	Cyan Laser Head with PC13302 Cyan Scientific Controller	Newport Corporation, Spectra Physics
APD	Model PD5CTC PDM Series	Micro Photon Devices
CCD	Andor iXon	Andor Technology
Reference Photo Diode	S2387	Hamamatsu
Laser Power Meter	Field Max II	Coherent
AdWin	AdWin Gold II	Jäger Computergesteuerte Messtechnik GmbH
Flow Cryostat	KONTI-Cryostat Micro	CryoVac
Temperature Controller	TIC 304 MA	CryoVac
Turbomolecular pump	PT70F-Compact	Leybold Vacuum
Turbomolecular pump system	EXT70	Edwards
	pre-pump E2M0.7	Edwards
Helium Pump	ME 4 NT	Vacuubrand

Table A.2.: *An overview over the equipment used to measure data.*

Component	Type	Manufacturer
Microscope Objective	LWD 50x/0.55/∞	Edmund Optics
SIL	Half Ball Lens Fused Silica N-BK7	Techspec/Edmund Optics
Filter	Cyan Laser Head with PC13302 Cyan Scientific Controller	Newport Corporation, Spectra Physics
Filter	Laser clean-up bandpass filter 483-493 nm	AHF Analysentechnik
Filter	Laser clean-up bandpass filter 320-340 nm	AHF Analysentechnik
Filter	Detection bandpass filter 525-725 nm	AHF Analysentechnik

Table A.3.: *The main optical components used.*

Overview over publications

Experiments on single triads

Chapter 5 covers the experiments shown in this publication.

Johannes Maier*, Martti Pärs*, Tina Weller, Mukundan Thelakkat and Jürgen Köhler: *Deliberate Switching of Single Photochromic Triads*, Sci. Reps. 7 (2017), 41739

Chapter 6 is the basis of a manuscript in preparation

Johannes Maier, Tina Weller, Mukundan Thelakkat and Jürgen Köhler: *Long-term stability of single photochromic triads based on dithienylcyclopentene photoswitches*

The manuscript will be submitted to a journal within the next month.

Experiments on ensembles of triads

I am a co-author of this publication. It is not covered in this dissertation, however, results contributed to the design and the measurements strategy for the experiments on single triads. These results are described and cited in section 3.5.

Johann Thurn*, Johannes Maier*, Martti Pärs, Katja Gräf, Mukundan Thelakkat, and Jürgen Köhler: *Temperature Dependence of the conversion efficiency of photochromic perylene bisimide dithienylcyclopentene triads embedded in a polymer*, Phys. Chem. Chem. Phys. 19 (2017), 26065-26071

*Equal contribution of the two authors

Erklärung

Hiermit versichere ich an Eides statt, dass ich die vorliegende Arbeit selbstständig verfasst und keine anderen als die von mir angegebenen Quellen und Hilfsmittel benutzt habe.

Ich erkläre, dass ich die vorgelegte Abhandlung nicht bereits zur Erlangung eines akademischen Grades eingereicht habe und dass ich keinerlei früheren Promotionsversuche unternommen habe.

Des weiteren erkläre ich, dass ich Hilfe von gewerblichen Promotionsberatern bzw. -vermittlern oder ähnlichen Dienstleistern weder bisher in Anspruch genommen habe noch künftig in Anspruch nehmen werde.

Bayreuth, den

. . . . . .

Johannes Maier